Use of Sun-Induced Chlorophyll Fluorescence in Linear and Nonlinear Light Use Efficiency Models for Remote Estimation of Plant Photosynthesis Under Stress Conditions

M. Pilar Cendrero-Mateo, Shari Van Wittenberghe, Valero Laparra, Uwe Rascher, Shirley A. Papuga, Guillermo Ponce-Campos, and Jose Moreno

***Abstract*—This study assessed the potential of sun-induced chlorophyll fluorescence (SIF) to estimate plant net photosynthesis (A_{net}) using a series of linear and nonlinear light-use efficiency (LUE) models. These models incorporated chlorophyll content-based vegetation indices as proxies for the fraction of absorbed photosynthetically active radiation (APAR) and nonphotochemical and photochemical quenching-related vegetation indices or reflected radiance based biophysical variables as proxies for LUE. A spectral unmixing technique was employed to retrieve the fluorescence quantum efficiency (FQE) and the flux of photons absorbed by beta-Carotene and xanthophyll pigments (APAR-CarbXan), key drivers of nonphotochemical quenching (NPQ). In this study, the maximum photosystem II efficiency (ΦPSII) ranged from 0.10 to 0.40, indicating a low level of photosynthetic performance under the observed conditions. In these conditions, the NPQ exhibited a high level of activation, which controlled the light reaction energy dissipation pathway and broke the positive linear relationship between photochemistry and fluorescence. Therefore, in this study, linear models incorporating FQE and APAR-CarbXan or their combination with meteorological variables failed to accurately capture the seasonal variations in A_{net}. However, the inclusion of a nonlinear relationship between LUE and FQE significantly improved model performance, demonstrating the necessity of nonlinear models for accurate SIF-based photosynthesis estimation.**

***Index Terms*—Light use efficiency (LUE) model, net photosynthesis, nonphotochemical quenching (NPQ), photosynthetically active radiation, sun-induced chlorophyll fluorescence (SIF).**

I. Introduction

THE process of photosynthesis is highly variable, with plants optimizing and regulating at different levels (e.g., canopy, leaf, and physiological level) [1]. The process of photosynthesis can be divided into three principal phases.

1) Primary reactions, which encompass the absorption and conversion of solar energy into electrical energy.
2) Light reactions, which entail the conversion of electrical energy into chemical energy.
3) Dark reactions, which facilitate the conversion of chemical energy into stable chemical energy in sugars [2] (see Fig. 1).

At the leaf level, light absorption depends on the composition of photosynthetic pigments and the internal leaf structure (see Fig. 1, left). At the physiological level, the efficiency with which the absorbed light energy is converted into biochemical energy and carbohydrates depends on the functional status of the light, the biochemical conversion of pigments involved in the photoprotective responses [3], [4], and the dark reactions (see Fig. 1, left). In particular, for the light responses, the absorbed photon energy can be assigned to photochemistry (or the rate of electron transport by photosystem II), dissipated as (nonconstitutive) thermal energy, widely referred to as nonphotochemical quenching (NPQ), or re-emitted as chlorophyll a fluorescence (ChlF) in the 640–850 nm spectral region [5], [6], [7]. For the dark reactions, the biochemical reactions (carbohydrate biosynthesis, photorespiration, and respiration) involved in the conversion of adenosine triphosphate (ATP) and nicotinamide

Received 11 September 2024; revised 10 December 2024, 7 February 2025, and 31 March 2025; accepted 14 April 2025. Date of publication 21 April 2025; date of current version 30 June 2025. The work of M. Pilar Cendrero-Mateo was supported by the Generalitat Valenciana grant project for the scientific excellence of junior researchers under Grant CISEJI/2023/48. The work of Shari Van Wittenberghe was supported by the European Research Council under the ERC-2021-STG under Grant 101041768. The work of Valero Laparra was supported by the Spanish Ministry of Science and Innovation under Project PID2020-118071GB-I00. The work of Shirley A. Papuga was supported by the NSF EAR MCA under Award 2126206. The work of Guillermo Ponce-Campos was supported by the USDA-ARS, Southwest Watershed Research Center. This work was performed within the German-Plant-Phenotyping Network which was supported by the German Federal Ministry of Education and Research under Project 031A053 and also by the Deutsche Forschungsgemeinschaft (German Research Foundation) under Germany's Excellence Strategy—EXC 2070—under Grant 390732324. *(Corresponding author: M. Pilar Cendrero-Mateo.)*

M. Pilar Cendrero-Mateo, Shari Van Wittenberghe, Valero Laparra, and Jose Moreno are with the Image Processing Laboratory, University of Valencia, 46980 Paterna, Spain (e-mail: m.pilar.cendrero@uv.es; shari.wittenberghe@uv.es; jose.moreno@uv.es).

Uwe Rascher is with the Institute of Bio- and Geosciences: Plant Sciences (IBG-2), Forschungszentrum Jülich GmbH, 52428 Jülich, Germany, and also with the University of Bonn: Faculty of Agricultural, Nutritional and Engineering Sciences, Institute of Crop Science and Resource Conservation, 53115 Bonn, Germany (e-mail: u.rascher@fz-juelich.de).

Shirley A. Papuga is with the Department of Environmental Science and Geology, Wayne State University, Detroit, MI 02445 USA (e-mail: shirley.papuga@wayne.edu).

Guillermo Ponce-Campos is with the School of Natural Resources and Environment, University of Arizona, Tucson, AZ 85719 USA (e-mail: geponce@arizona.edu).

This article has supplementary downloadable material available at https://doi.org/10.1109/JSTARS.2025.3562256, provided by the authors.

Digital Object Identifier 10.1109/JSTARS.2025.3562256

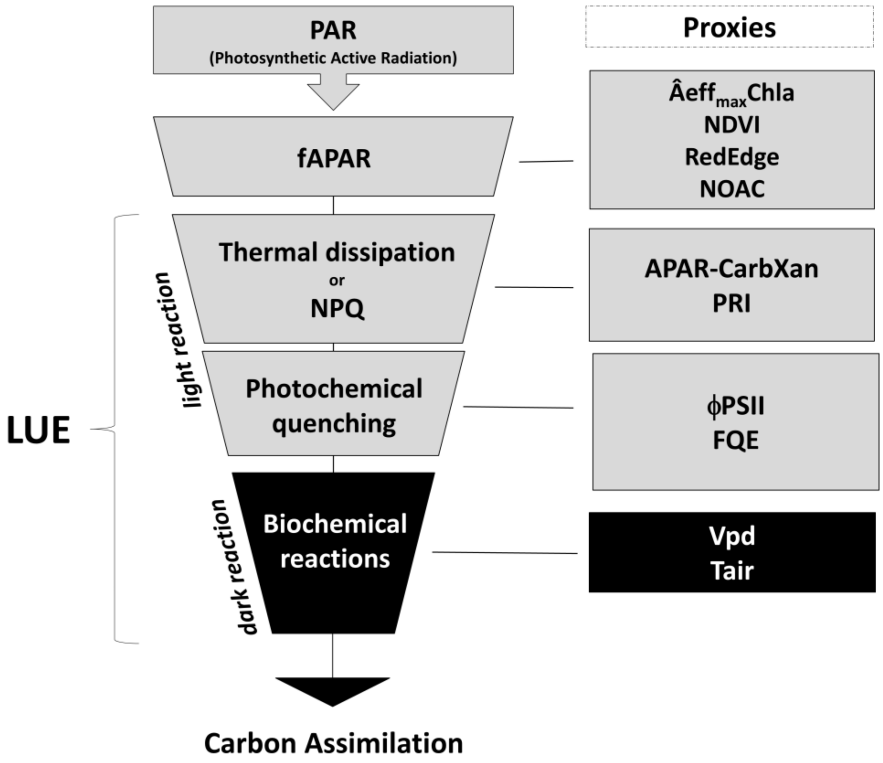

Fig. 1. Following diagram illustrates the methodology employed in this paper to estimate photosynthesis. In accordance with the light-use-efficiency model proposed by Monteith, the estimation of photosynthesis is based on three key variables: (1) the fraction of the photosynthetically active radiation absorbed by vegetation (fAPAR), (2) light use efficiency (LUE), which represents the conversion efficiency of absorbed energy to carbon assimilation, and (3) correction factors related to meteorological conditions that limit LUE. In this manuscript, the Chla effective absorbance ($\hat{A}eff_{max}Chla$), Normalized Difference Vegetation Index (NDVI), RedEdge index, and normalized Area Over Reflectance Curve index (NAOC) are employed as proxies for fAPAR. (ii) Photon flux absorbed by beta-Carotene and xanthophyll pigments (APAR-CarbXan) and the Photochemical Reflectance Index (PRI) are employed as proxies for thermal energy dissipation, which is widely addressed as non-photochemical quenching (NPQ). (iii) Quantum yield of photochemical energy conversion (ΦPSII) and fluorescence quantum yield (FQE) are employed as proxies for photochemical quenching, or the rate of electron transport through ΦPSII. Furthermore, vapor pressure deficit (Vpd) and air temperature (Tair) serve as the meteorological conditions that regulate the opening of stomata, thereby influencing the biochemical reactions (carbohydrate biosynthesis, photorespiration, and respiration) involved in the conversion of ATP and NADH to sugars and carbon assimilation during the dark reactions. The scheme was adapted from the ESA Fluorescence Explore (FLEX) mission consultation meeting, which took place on 15—16 September 2015, in Krakow, Poland.

adenine dinucleotide phosphate into sugars are those that limit the photosynthetic efficiency of plants.

The widely discussed NPQ is a set of processes actively developed by plants that protect vegetation from photodamage by dissipating excess light energy as heat. NPQ is a complex phenomenon involving multiple biochemical (i.e., synthesis or breakdown of specific molecules) and biophysical (i.e., light absorptions, energy transfer, or proteins structural changes) processes, likely occurring at various quenching sites within the photosynthetic apparatus [8], [9], [10], [11], [12], [13], [14], [15], [16], [17]. An important role in this energy quenching is played by the carotenoid's pigments—beta-carotene and xanthophyll. When these carotenoids interact with excited chlorophyll molecules, they can accept the excess energy and transfer it to vibrational energy, which is then dissipated as heat [18]. At the same time, chlorophyll fluorescence plays a crucial role in protecting plants from photooxidative damage. By emitting excess light energy that is not dissipated as NPQ through fluorescence, plants can safely dissipate harmful energy that could otherwise cause damage to photosynthetic components.

Most studies evaluating the estimation of photosynthesis are based on the following.

1) Mechanistic models: where photosynthesis rate is a function of absorbed photosynthetically active radiation (APAR), leaf temperature, intercellular CO_2 concentration, and Rubisco enzyme activity [2], [19].
2) Statistical models: these establish statistical correlations between remote sensing data [mainly vegetation indices (VIs) and sun-induced chlorophyll fluorescence (SIF)], environmental factors, and ground-based measurements of vegetation productivity using regression trees, neural networks, and other complex statistical methods [2], [20].
3) Semi-empirical models such as the light use efficiency (LUE) model ([21], [22], where three key variables constrain the photosynthetic capacity of the plant, namely

a) the fraction of photosynthetically active radiation absorbed by leaves (FAPAR);
b) LUE, which represents the efficiency of converting absorbed energy into fixed carbon;
c) correction factors related to meteorological conditions that limit LUE. The present study will focus on LUE-based models.

Direct and noninvasive measurements of FAPAR and LUE are difficult to obtain. Previous studies have developed methods to

estimate FAPAR and LUE using proxies. Structure-related optical VIs such as normalized difference vegetation index (NDVI) and RedEdge index have been used as proxies for FAPAR [23], [24], [25]. Physiologically related parameters, such as photochemical reflectance index (PRI) and SIF, have been used as proxies for LUE [26], [27]. In addition, recent studies have taken advantage of the high spectral resolution of the proximal benchmark sensors to quantify, based on spectral unmixing techniques, the fluorescence quantum efficiency (FQE), defined as the ratio of fluorescence photons emitted by chlorophyll to the flux of absorbed photons, or APAR-Chla; as well as the flux of photons absorbed by the carotenoid pigments—beta-Carotene and xanthophyll (APAR-CarbXan)—linked to the NPQ mechanisms [4], [28].

The PRI index [29] and the APAR-CarbXan [30] have been employed to monitor variations in the reflectance spectrum associated with rapid xanthophyll pool variations or long-term changes in the constitutive chlorophyll and carotenoids pools, as well as temporal variations in NPQ [31], [32]. With regard to fluorescence, a strong linear correlation between fluorescence and photochemistry has been observed in a variety of ecosystems, including forests [27], [33], [34] and agricultural areas [35]. This is due to the fact that fluorescence and photochemistry are linked through the actual amount of light absorbed by chlorophyll molecules. Nevertheless, recent studies have demonstrated that this positive correlation is valid for a specific period during which LUE can be assumed to be constant [36], [37]. However, plants are frequently subjected to stressful conditions, including those induced by light (diurnal cycle), limited resources (water or nutrients), temperature (heat or cold wave), or even the combination of several factors [38]. In such circumstances, the various NPQ mechanisms are triggered, resulting in an increase in the energy dissipation pathway and the disruption of the linear relationship between photochemistry and fluorescence [39].

The objective of this study was to investigate the intertwined dynamics of energy dissipation altering the linear relationship between photochemistry and fluorescence. To this end, the study was designed to assess the seasonal trends and relationships observed between photosynthesis, FAPAR, and LUE-related proxies (i.e., optical vegetation indices, nonphotochemical quenching, and chlorophyll fluorescence), all of which were measured at the leaf level in a well-watered wheat field growing under suboptimal nitrogen treatments. The objective of this study was to evaluate the contribution of SIF and competing energy dissipation mechanisms to linear and nonlinear light-use efficiency-based models for the remote estimation of plant photosynthesis.

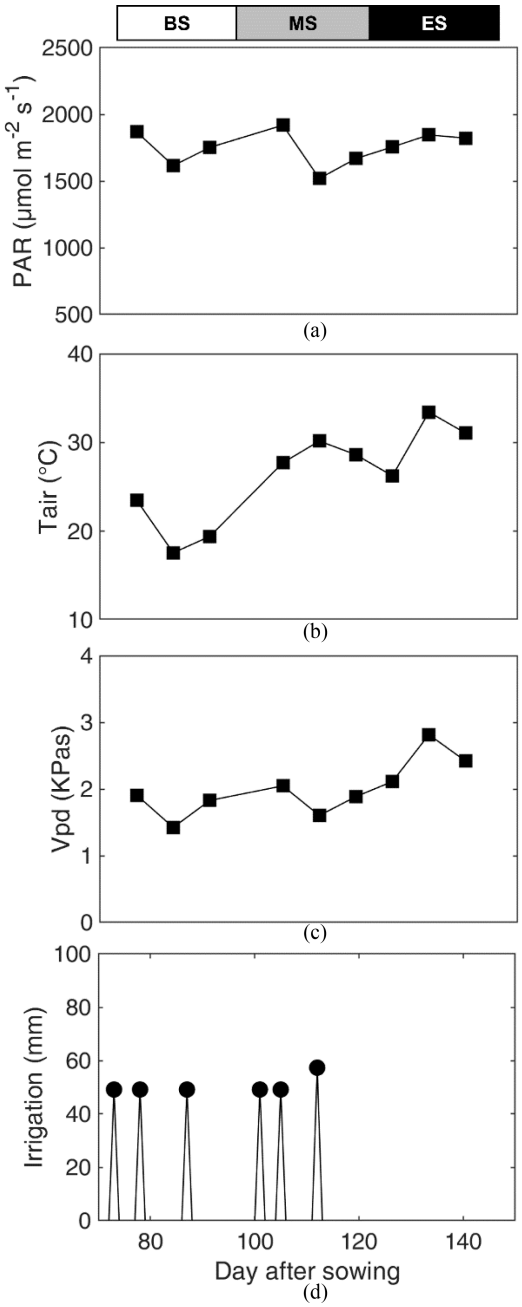

Fig. 2. Seasonal variation of photosynthetic active radiation (PAR), air temperature (Tair), vapor pressure deficit (Vpd), and irrigation regimes. The three seasonal periods described in the manuscript are the beginning of the season (days after sowing (DAS) 77 to 91, BS), the middle of the season (DAS 105 to 119, MS), and the end of the season (DAS 126 to 140, ES). This aligns with the wheat growth stages of jointing (BS), heading and anthesis (MS), and grain filling (ES).

II. Material and Methods

A. Field Experiment

A winter durum wheat experiment was conducted at the University of Arizona's Maricopa Agricultural Center in Arizona, USA. Daily meteorological variables [i.e., solar radiation, air temperature (T_{air}), and vapor pressure deficit (Vpd)] for this study site were available from the Maricopa Arizona Meteorological Station[1] (see Fig. 2), which is located 500 m from the experimental field, minimizing the potential for significant discrepancies in meteorological conditions such as temperature, solar radiation, and wind speed. A split-plot design with three replications of *Triticum durum* cv. Orita under three nitrogen fertilizer application rates was used for the experiment: low nitrogen treatment (0 kg/ha, LN), medium nitrogen treatment (90 kg/ha, MN), and high nitrogen treatment (202 kg/ha, HN). The specific nitrogen levels were chosen based on previous experimental results [40].

[1][Online]. Available: http://ag.arizona.edu/azmet/

After two months of plant growth (i.e., beginning of tillering), coincident measurements of gas exchange, active fluorescence, reflectance, and passive fluorescence were made on the same leaves under the same environmental conditions once a week for nine measurement days from 24 February to 27 April. Measurements were always conducted under clear sky conditions during the morning hours (09:00 to 11:00). Each day, three fully expanded flag leaves exposed to direct sunlight were selected per replicate and treatment (number of leaves per treatment and day = 9, total number of leaves per day = 27). At the beginning (day after sowing 93), middle (day after sowing 113), and end (day after sowing 133) of our measurement period we collected total dry weight biomass (leaf, stem and boot—kg/ha). Flag leaves were selected for measurement because they are the largest, most photosynthetically active leaves [41], and their position minimizes shading and maximizes photosynthetic rates. More details about this experiment can be found in [42].

Based on the days after sowing (DAS), three seasonal periods were identified: early season (BS: DAS 77 to 91), mid season (MS: DAS 105 to 119), and late season (ES: DAS 126 to 140). These seasons are intended to correspond to the wheat growth stages of jointing (BS), heading and anthesis (MS), and grain filling (ES).

B. Net Photosynthesis Measurements

Seasonal measurements of A_{net} and stomatal conductance (gs) at the leaf level were made using a gas exchange system equipped with an infrared gas analyzer (Licor 6400-40XT leaf chamber fluorometer, Li-COR Biosciences, Lincoln, NE, USA). These measurements were taken under ambient field conditions of irradiance, temperature, and humidity. Leaves were maintained in the assimilation chamber under constant ambient CO_2 concentration (400 μmol mol^{-1}). Measurements were taken when A_{net}, gs, and internal CO_2 reached steady state conditions.

C. Chlorophyll Fluorescence Measurements

Active chlorophyll fluorescence measurements were performed simultaneously as A_{net} using a Licor 6400-40XT leaf chamber fluorometer (Li-COR Biosciences, Lincoln, NE, USA). Pulse amplitude modulated (PAM) fluorometry measurements included light-adapted steady-state fluorescence (F_s), maximum light-adapted fluorescence ($F_{m'}$), and maximum photosystem II efficiency ($\Phi\text{PSII} = 1 - F_s / F_{m'}$), where ΦPSII provides an estimate of the actual efficiency of photosystem II photochemistry at a given photosynthetically active radiation (PAR) [43].

Passive chlorophyll fluorescence measurements were also performed consecutively on the same leaves as A_{net} and active fluorescence by coupling a spectroradiometer to the FluoWat leaf clip [44]. The ASD FieldSpec point spectroradiometer (Analytical Spectral Devices, Boulder, CO, USA) was used with a spectral range between 350 and 2500 nm and a full width half maximum of 3 and 10 nm in the 350–1050 and 1050–2500 nm regions, respectively. With the FluoWat leaf clip it is possible to measure the entire chlorophyll fluorescence emission spectrum by blocking the incident light spectrum with a short pass filter (<650 nm). At wavelengths longer than 650 nm, only SIF emission is recorded, as light in this region is only emitted light. The FluoWat leaf clip also allows the measurement of leaf reflectance (R) and leaf transmittance (T) by placing the ASD fiber in either an up or down position. In addition, total solar irradiance (I) was measured before and after each leaf measurement using a spectralon panel (ODM-98, Gigahertz-Optik GmbH, Türkenfeld, Germany) together with the FluoWat. The total FAPAR was calculated based on the R and T measurements between 400 and 700 nm, without differentiating between the pigment fractions of absorbed PAR

$$\text{FAPAR} - \text{fluowat} = \int_{400}^{700} A \cdot d_\lambda = \int_{400}^{700} (1 - R - T) \cdot d_\lambda \tag{1}$$

where A is the fraction of light absorbed by the leaf and d_λ is the wavelength dependence.

To disentangle the light absorbed by the different energy dissipation pathways (including chlorophyll and the carotenoids associated with NPQ) and to estimate FQE, a pigment spectral unmixing technique recently described by [28] was applied. In essence, the calculated effective absorbance ($\hat{A}\text{eff}_{\max}$) of individual pigments, including chlorophyll a ($\hat{A}\text{eff}_{\max}$Chla), chlorophyll b ($\hat{A}\text{eff}_{\max}$Chlb), beta-carotene ($\hat{A}\text{eff}_{\max}$b-Car), and xanthophylls ($\hat{A}\text{eff}_{\max}$Xan), was derived through the application of a non-negative least squares (NNLS) linear spectral unmixing approach, which was based on the absorption characteristics of the pigments [28]. The FQE was calculated as the ratio of the total fluorescence energy emitted in both upward and downward directions (see Fig. S1, Supplementary material) to the total energy absorbed by Chla [APAR-Chla, Fig. 3(d)]. The latter was determined by multiplying the effective absorbance of Chla by the measured total irradiance. To calculate the total photon flux absorbed by carotenoid pigments (i.e., beta-Carotene and xanthophylls), their respective effective absorbances were multiplied by the measured solar irradiance at leaf level, with their sum yielding APAR-CarbXan.

In addition, other optical vegetation indices related to chlorophyll concentration and light use efficiency were calculated from the leaf reflectance spectra. These are the NDVI index [NDVI = (R830–R670)/(R830+R670), [45]] the RedEdge index (RedEdge = R750/R710, [46], [47]) the normalized area over reflectance curve index (NAOC = $1 - (\int_{643}^{795} R\, d\lambda)/(152 \cdot R795)$, [48]), and the PRI index (PRI = (R531–R570)/(R531+R570), [29]). Finally, the LUE was calculated based on the A_{net} measurements of the Licor 6400 and the APAR-Chla retrieved from the Fluowat dataset (LUE = A_{net}/APAR-Chla).

D. Light Curve Measurements

Gas exchange and chlorophyll fluorescence measurements were conducted using a Li-Cor 6400XT (Li-Cor Biosciences, Lincoln, NE, USA) portable photosynthesis system equipped with a 6400-40 leaf chamber fluorometer. This system employs a light source consisting of independently controlled LEDs (three blue, one far-red, and one red). A reference CO_2 concentration of 380 μmol mol^1 was maintained by mixing CO_2-depleted air with CO_2 from a gas cylinder. Leaf temperature was kept constant at 25 °C, and a 2 cm^2 leaf area was enclosed within the

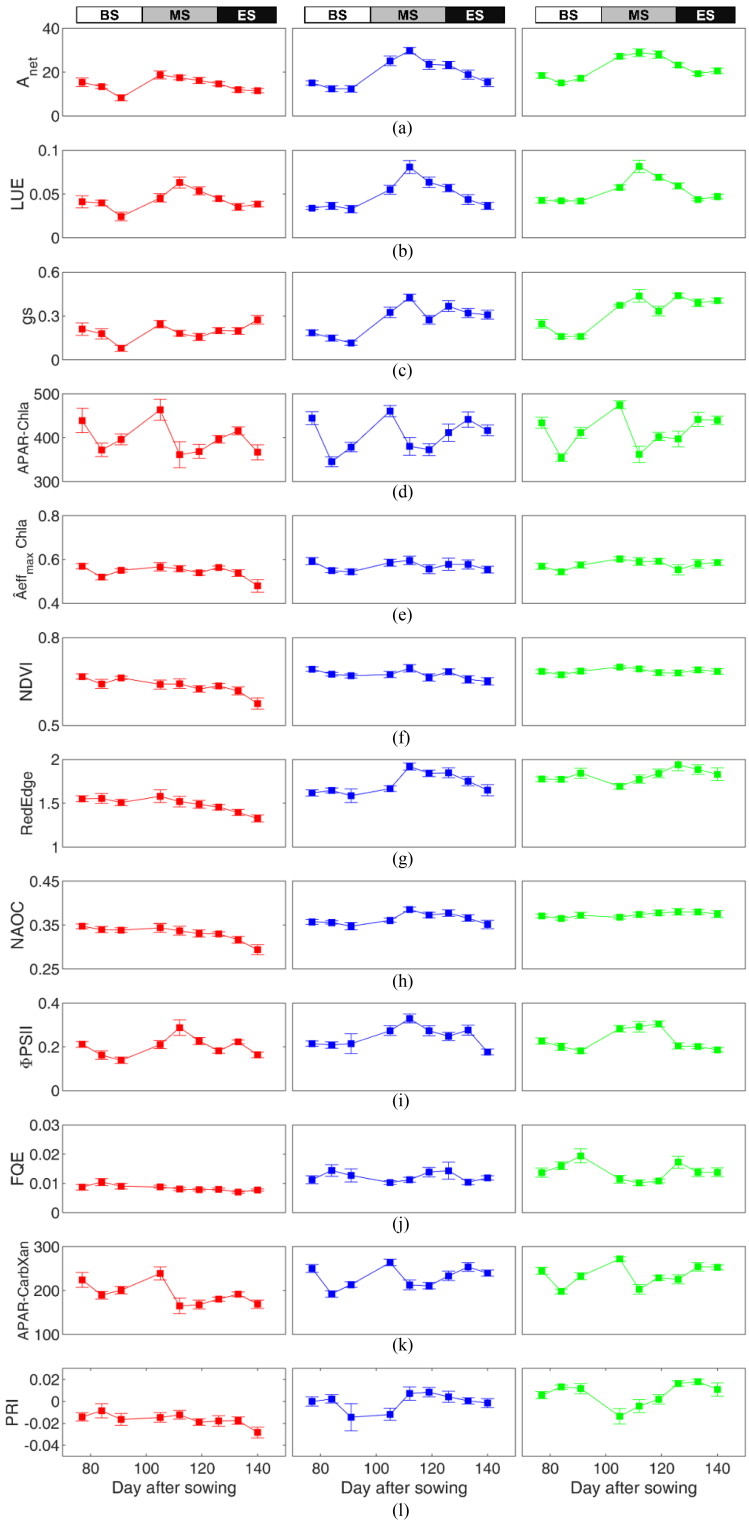

Fig. 3. Seasonal variation of net photosynthesis (A_{net}, μmol CO_2 m^{-2} s^{-1}), light use efficiency (LUE $= A_{\text{net}}$/APAR-Chla, $\frac{CO_2}{\text{photons}}$), stomatal conductance (gs, μmol HO_2 m^{-2} s^{-1}), absorbed photosynthetic active radiation by Chla molecules (APAR-Chla, μmol m^{-2} s^{-1}), Chla effective absorbance ($\hat{A}\text{eff}_{\max}$Chla, -), Normalized Difference Vegetation Index (NDVI, -), RedEdge index (RedEdge, -), normalized Area Over Reflectance Curve index (NAOC, -), quantum yield of photochemical energy conversion (ΦPSII, -), fluorescence quantum yield (FQE, $\frac{\text{photons emitted}}{\text{photons absorbed}}$), photon flux absorbed by beta-Carotene and xanthophyll pigments (APAR-CarbXan, μmol m^{-2} s^{-1}) and the Photochemical Reflectance Index (PRI, -) in wheat plants grown under low (red), medium (blue), and high nitrogen (green) conditions. The three seasonal periods described in the manuscript are the beginning of the season (days after sowing (DAS) 77 to 91, BS), the middle of the season (DAS 105 to 119, MS), and the end of the season (DAS 126 to 140, ES). This aligns with the wheat growth stages of jointing (BS), heading and anthesis (MS), and grain filling (ES). Number of replicates, $n = 9$ per day. Error bars represent standard deviation within replicates for each day and treatment.

sample cuvette. Dark-adapted fluorescence and gas exchange measurements were performed before the onset of the photoperiod (5:00 A.M.). Subsequently, light-adapted measurements were initiated four hours later (9:00 A.M.) and completed within approximately six hours. The same leaf from each plant was used for both dark- and light-adapted measurements. Light-response curves were generated by systematically varying the incident PAR levels from 1800 to 0 μmol m^2 s^1, simulating the transition from darkness to peak midday illumination. Leaves were allowed to acclimate for 1–4 min at each PAR level, with longer acclimation times required for lower and higher PAR levels. Measurements were taken when A_{net}, gs, and internal CO_2 reached steady-state conditions. To validate the measurement procedure, light-response curves were also measured on some plants with PAR levels increasing incrementally from 0 to 1800 μmol m^2 s^1. Chlorophyll fluorescence parameters measured included minimum fluorescence in the dark (F_o), F_s and both light- and dark-adapted maximum fluorescence (F_m, F_m'). ΦPSII and nonphotochemical quenching (NPQ = (F_m–F_m')/F_m) were derived from F_s, F_m, and F_m' measurements respectively. Maximum fluorescence yield was achieved by exposing the leaf to a two-second saturating light flash (8000 μmol m^2 s^1).

E. Linear Modeling Approach: Monteith's Light-Use-Efficiency

Three alternative approaches were employed to test the efficacy of Monteith's linear LUE model (GPP = LUE×FAPAR×PAR). In each approach, different parameters were evaluated as potential proxies for LUE and FAPAR (see Fig. 1). In this study, LUE includes the different pathways that plants use for photoprotection, such as nonphotochemical and photochemical quenching mechanisms, and the interdependence between light and dark reactions (see Fig. 1). It should be noted that, given that this study employed the measurement of net photosynthesis at the leaf level, the term A_{net} is used instead of GPP. The models were evaluated in three ways. First, they were evaluated based on the complete data set, which is subsequently described as "All" in figures and tables. Second, they were evaluated based on data collected at the BS, MS, and ES, without discriminating between nitrogen treatments. Third, they were evaluated based on the impact of the treatment (LN, MN, and HN), without differentiating between seasonal periods.

Approach 1: Meteorology-driven methods (MM). In this approach, NDVI was used to explain the variability of FAPAR with the season and $T\text{min}_{\text{scalar}}$ and $V\text{pd}_{\text{scalar}}$ as the limiting factor of the maximum LUE (LUE_{max}). Monteith's LUE model was reformulated as follows:

$$A_{\text{net}} = [\text{LUE}_{\text{max}} \cdot T\text{min}_{\text{scalar}} \cdot V\text{pd}_{\text{scalar}}] \times [(a_0 + \text{NDVI} \cdot a_1) \cdot \text{PAR}] \quad (2)$$

where LUE_{max}, a_0, and a_1 are model parameters and $T\text{min}_{\text{scalar}}$ (scalar minimum temperature) and $V\text{pd}_{\text{scalar}}$ [scalar vapor pressure deficit (Vpd)] are simple linear ramp functions of daily minimum temperature and Vpd as described at the MODIS user guide MOD17A2/A3 [49]. In this approach, two alternatives were tested, 1) where NDVI was used as a proxy for FAPAR and 2) where the terms "$(a_0 + \text{NDVI} \cdot a_1) \cdot \text{PAR}$" were replaced by APAR-Chla.

Approach 2: Remote sensing based method (RSM) [50]. Based on the reformulation of Monteith's LUE model as follows:

$$A_{\text{net}} = \text{LUE} \cdot \text{FAPAR} \cdot \text{PAR} = (a_0 \cdot \text{Ph} + a_1) \times (a_2 \cdot \text{St} + a_3) \cdot \text{PAR}. \quad (3)$$

Fifteen alternatives were obtained from the combination of PRI, FQE, and APAR-CarbXan as physiological (Ph) proxies for LUE and NDVI, RedEdge, NAOC, $\hat{A}\text{eff}_{\text{max}}$Chla, and as structural (St) proxies for FAPAR. Similar to the previous approach, the terms "$(a_2 \cdot \text{St} + a_3) \cdot \text{PAR}$" were replaced by APAR-Chla. In (3), a_0, a_1, a_2, and a_3 are fitting parameters.

Approach 3: Following the conceptual framework of Berry et al. [51], who suggested using the PAM-derived fluorescence yield (ΦFPSII), equivalent to the ΦPSII measured in this study, to investigate the mechanisms controlling SIF and LUE during steady-state photosynthesis, in this approach the Monteith's LUE model was reformulated as follows:

$$A_{\text{net}} = \text{LUE} \cdot \text{FAPAR} \cdot \text{PAR} = a_0 \cdot (\text{LUE} \cdot \text{FAPAR} \cdot \text{PAR}) = a_0 \cdot (\Phi\text{PSII} \cdot \text{Opt} \cdot \text{PAR}) \quad (4)$$

where five alternative formulations with optical proxies (Opt) were obtained from the combination of the NDVI, RedEdge, NAOC, $\hat{A}\text{eff}_{\text{max}}$Chla, and as structural related (St) as FAPAR proxy. Similar to the previous approach, the terms "Opt ċ PAR" were replaced by APAR-Chla. In this approach ΦPSII was used as the LUE proxy. In (4), a_0 is a fitting parameter.

In all three approaches described above, a linear relationship was assumed between LUE, FAPAR and the parameters used to explain their seasonal variability.

F. Nonlinear Modeling Approach: Gaussian Regression Light-Use-Efficiency Based Models

The estimation of biophysical parameters has been approached using either statistical, physical, or hybrid methods [52]. This section is focused on statistical approximations. Statistical methods can be either parametric or nonparametric. Parametric models use the knowledge of plant physiological processes to construct explicit parameterized expressions to explain variation in A_{net}. Alternatively, nonparametric models are fitted to predict a variable of interest using a training dataset of input–output data pairs derived from simultaneous measurements of the parameter of interest (A_{net}) and the corresponding independent parameters observations (e.g., optical vegetation indices, fluorescence, and meteorological parameters).

In previous publications, the nonparametric Gaussian process regression (GPR) model has shown excellent results in the estimation of leaf chlorophyll content, leaf area index, and fractional canopy cover from remotely sensed images [53], [54], [55]. GPR is much more flexible than the models in the previous sections, as it builds a nonlinear regression model using the observed parameters (i.e., physiological and meteorological) as inputs

and without considering physical constraints. Here, based on the input parameters of light use efficiency, GPR was used as a tool to infer the amount of information that each combination of optical vegetation indices, ΦPSII, FQE, APAR-CarbXan, and meteorological parameters (i.e., V_{pd} and T_{air}) contains about A_{net}. A total of 308 models were evaluated (Supplementary material spreadsheet GPR models results), for more information on GPR parameterization see [53] and [55]. The objective was to develop a nonparametric model for each potential combination of FAPAR or APAR (i.e., NDVI, RedEdge, NAOC, $\hat{\mathrm{A}}\mathrm{eff}_{\mathrm{max}}\mathrm{Chla}$, APAR-Chla), LUE (i.e., ΦPSII, FQE, APAR-CarbXan), and meteorological conditions (i.e., V_{pd} and T_{air}) input variables. The contribution of each input variable to the prediction was analyzed.

G. Statistical Analysis and Model Performance

As previously described, the models were evaluated based on the complete dataset (later referred to as All in figures and tables), considering only the data collected at BS, MS, and ES, as well as the effect of treatment (LN, MN, and HN) on the seasonal dynamics of photosynthesis. For all model combinations, the available data were randomly divided into half sets: 50% samples for training and 50% samples for testing performance. Each model was repeated ten times for ten randomly selected training and test data sets, and then the average results were reported. Statistical analyses were performed using MATLAB 2023a (MathWorks Inc., Natick, USA) and the R standard package (R version 0.98.994, R Development Core Team, 2014). To evaluate the performance efficiency of linear and nonlinear LUE models and to ensure a fair comparison between them, a series of statistical indices were employed. All three linear (MM, RMS, and Berry-based) and non-linear LUE models were evaluated for 1) accuracy, where the coefficient of determination (R^2) and bias ($\sigma_{(A\mathrm{net\text{-}predicted} - A\mathrm{net\text{-}measured})}$) explained the difference between the expected prediction of the model and the actual value, and 2) precision or variance ($\mu_{(A\mathrm{net\text{-}predicted} - A\mathrm{net\text{-}measured})}$), which explained the variability of a model prediction for a given data point. In addition, the p-value and Akaike's information criterion (AIC, [56]) were calculated. The model with the lowest AIC was considered the best among the different model formations.

Furthermore, one-way analysis of variance (ANOVA) was employed to evaluate statistical differences in total biomass, A_{net}, and the various parameters utilized as proxies for FAPAR and LUE between treatments (see Table I) (IBM SPSS Statistics, version 26.0). Student's t-tests were utilized to compare the groups LN, MN, and HN. Normality and homogeneity of variance assumptions were verified through Shapiro-Wilk and Levene's tests, respectively. Statistical significance was determined at the $\alpha = 0.05$ level.

III. Results

Following the objectives of this study, an initial analysis of the seasonal changes observed in meteorological conditions, net photosynthesis, optical vegetation indices and chlorophyll fluorescence within and between treatments was conducted. Second, the performance of linear and nonlinear LUE models estimating net photosynthesis, as well as the contribution of the different parameters considered in this study is described.

A. Seasonal Dynamics Changes of Net Photosynthesis, Optical Vegetation Indices, and Chlorophyll Fluorescence

The Maricopa Arizona Meteorological Station recorded constant photosynthetically active radiation (PAR) values between 1500 and 1900 μmol m^{-2} s^{-1} throughout the course of the experiment. During the measurement period, both T_{air} and V_{pd} exhibited an increase, reaching a maximum of 33 °C and 3 kPa (DAS 133) and a minimum of 17 °C and 1.5 kPa (DAS 84), respectively. Irrigation regimens were consistently applied at a rate of ∼50 mm per application, occurring at regular intervals, and ceased on DAS 112 (see Fig. 2).

Clear seasonal trends of A_{net} and LUE were observed for low, medium, and high nitrogen treatments (LN, MN, and HN, respectively). A gradual increase was observed from the BS to MS, with the greatest increase occurring in MN and HN. Thereafter, a decrease was observed toward the ES [see Fig. 3(a) and (b)]. A similar pattern was observed in the case of *gs*, exhibiting a similar trend as that observed in A_{net} and LUE from the BS to the MS. However, towards the ES, *gs* exhibited a relatively constant value of approximately 0.3 μmol HO_2 m^{-2} s^{-1} [see Fig. 3(c)].

As expected, APAR-Chla followed a similar pattern to that of the PAR described. Where the PAR variability within the 09:00–11:00 measurement time interval is less than 10% (see Fig. S3, Supplementary material). Driven by the availability of nitrogen, from the BS to the MS, the MN and the HN presented slightly higher values than the LN. Toward the ES, MN, and HN showed higher values than LN [see Fig. 3(d)]. The differences between the nitrogen treatments (LN versus MN-HN) are more pronounced for $\hat{\mathrm{A}}_{\mathrm{effmax}}\mathrm{Chla}$ and the VIs used as a proxy for FAPAR (i.e., NDVI, RedEdge, and NAOC) [see Fig. 3(e)–(h)], where for most of the VIs and measurement periods, LN $<$ MN $<$ HN and/or LN $<$ MN-HN (p-value < 0.05, Table I). However, the seasonal patterns reflect subtle variations between measurement days. The RedEdge index is the VI which shows a clearer seasonal pattern, presenting a rising trend from the BS to the MS, and later, a slight decrease towards the ES. It is interesting to note that a comparison of the Chla/Chlb ratio [see Fig. S1(a), Supplementary material] between treatments revealed that, while the LN Chla/Chlb ratio increased throughout the season, the Chla/Chlb ratio of MN and HN treatments remained constant. Furthermore, the LN Chla/Chlb ratio was found to be significantly higher than those of MN and HN treatments (p-value < 0.05, data not shown).

The seasonal dynamics observed in ΦPSII were comparable to those observed in A_{net} [see Fig. 3(i)]. The values of ΦPSII ranged from 0.10 to 0.40, indicating a low level of photosynthetic performance. FQE, for MN and HN, exhibited opposite trends in comparison to ΦPSII and A_{net} [see Fig. 3(j)]. This is particularly evident in the case of HN-MS, where the lowest values of FQE coincide with the seasonal peak of ΦPSII and A_{net}. For LN, FQE remained constant throughout the season. For all treatments and across the seasonal measurements, comparable trends were observed between active (*Fs* and *Fm*') and passive

TABLE I
RESULTS OF THE REPEATED-MEASURES ANOVA F-TEST WHICH WAS CONDUCTED TO COMPARE THE EFFECTS OF NITROGEN TREATMENT (LOW (LN), MEDIUM (MN), AND HIGH (HN)) AT DIFFERENT SEASONAL PERIODS, THE COMPLETE SEASON (ALL), THE BEGINNING OF THE SEASON (DAYS 77 TO 91, BS), THE MIDDLE OF THE SEASON (DAYS 105 TO 119, MS), AND THE END OF THE SEASON (DAYS 126 TO 140, ES), ON TOTAL DRY WEIGHT BIOMASS, NET PHOTOSYNTHESIS (A_{NET}), ABSORBED PHOTOSYNTHETICALLY ACTIVE RADIATION BY CHLA MOLECULES (APAR-CHLA), CHLA EFFECTIVE ABSORBANCE ($\hat{A}EFF_{MAX}$CHLA), NORMALIZED DIFFERENCE VEGETATION INDEX (NDVI), REDEDGE INDEX (REDEDGE), NORMALIZED AREA OVER REFLECTANCE CURVE INDEX (NAOC), QUANTUM YIELD OF PHOTOCHEMICAL ENERGY CONVERSION (ΦPSII), FLUORESCENCE QUANTUM YIELD (FQE), PHOTON FLUX ABSORBED BY BETA-CAROTENE AND XANTHOPHYLLS PIGMENTS (APAR-CARBXAN), AND PHOTOCHEMICAL REFLECTANCE INDEX (PRI)

		Days			
Index	**Nitrogen**	**All**	**BS**	**MS**	**ES**
Total Biomass (Kg/ha)	**LN**	5551[a-b]	2338[a]	4814[a]	8698[a]
	MN	12239[b]	5561[b]	9009[b]	20479[b]
	HN	16599[b]	6432[b]	11945[b]	28878[b]
A_{net}	**LN**	14.17[a]	13.92[a]	16.13[a]	11.74[a]
	MN	19.52[b]	16.25[a]	25.51[b]	17.08[b]
	HN	22.00[b]	19.50[b]	26.99[b]	19.97[b]
APAR-Chla	**LN**	344[a]	379[a]	310[a]	323[a]
	MN	406[b]	407[a-b]	388[b]	429[b]
	HN	413[b]	419[b]	387[b]	441[b]
$\hat{A}eff_{max}Chla$	**LN**	0.54[a]	0.55[a]	0.55[a]	0.51[a]
	MN	0.57[b]	0.57[a]	0.58[a]	0.57[b]
	HN	0.58[b]	0.57[a]	0.58[a]	0.58[b]
NDVI	**LN**	0.63[a]	0.65[a]	0.63[a]	0.60[a]
	MN	0.67[b]	0.68[b]	0.68[b]	0.65[b]
	HN	0.69[c]	0.69[b]	0.68[b]	0.69[c]
RedEdge	**LN**	1.49[a]	1.55[a]	1.49[a]	1.36[a]
	MN	1.73[b]	1.63[b]	1.87[b]	1.70[b]
	HN	1.82[c]	1.77[c]	1.85[b]	1.86[c]
NAOC	**LN**	0.33[a]	0.34[a]	0.33[a]	0.31[a]
	MN	0.36[b]	0.36[b]	0.38[b]	0.36[b]
	HN	0.37[c]	0.37[c]	0.38[b]	0.38[c]
ΦPSII	**LN**	0.20[a]	0.18[a]	0.23[a]	0.19[a]
	MN	0.25[b]	0.23[b]	0.28[b]	0.23[a]
	HN	0.23[b]	0.22[b]	0.27[b]	0.19[a]
FQE (x100)	**LN**	0.84[a]	0.93[a]	0.80[a]	0.74[a]
	MN	1.23[b]	1.22[b]	1.31[b]	1.12[b]
	HN	1.40[c]	1.52[c]	1.27[b]	1.38[b]
APAR-CarbXan	**LN**	192[a]	213[a]	171[a]	180[a]
	MN	230[b]	230[a-b]	219[b]	247[b]
	HN	235[b]	237[b]	219[b]	254[b]
PRI (x100)	**LN**	-1.65[a]	-1.35[a]	-1.64[a]	-2.30[a]
	MN	-0.06[b]	-0.60[b]	0.65[b]	-0.06[b]
	HN	0.65[c]	0.41[c]	0.45[b]	1.43[c]

(FQE) measurements, thereby demonstrating the robustness of the experimental design [see Fig. S1(b) and (c), Supplementary material].

APAR-CarbXan manifested a dual pattern with respect to ΦPSII and A_{net}, presenting a comparable trend from DAS 77-105, followed by an inverse pattern from DAS 112-126, and then again, a similar trend toward the end of the experiment [see Fig. 3(k)]. As with FQE, a pronounced decline in APAR-CarbXan was noted when the maximum value of ΦPSII was reached. Finally, PRI and FQE for LN showed slight fluctuations throughout the season [see Fig. 3(l)]. Regarding MN and HN, the PRI seasonal pattern shows an initial increase (BS), followed by a decline (MS), and then a subsequent rise (ES). However, despite the described pattern follows an inverse trend compared to ΦPSII and A_{net}, at the MS the patterns appear to diverge from the ΦPSII and A_{net}, exhibiting a decrease prior to the increase of ΦPSII (MN and DAS 91) and an increase prior to the decrease of ΦPSII (HN and DAS 112). Finally, for most of the parameters used as LUE proxies and measuring periods, LN $<$ MN $<$ HN and/or LN $<$ MN-HN (p-value < 0.05, Table I).

The parameters derived from active fluorescence measurements taken during midseason demonstrate the dynamic response between F_s, ΦPSII, and NPQ, A_{net} (see Fig. 4). Analysis of the relationship between F_s and ΦPSII indicated the presence of two distinct trends [see Fig. 4(a)]. 1) A negative correlation was observed between F_s and ΦPSII at low (0.10–0.30) and high (0.60–0.80) values of ΦPSII, and 2) a positive correlation was observed at intermediate values

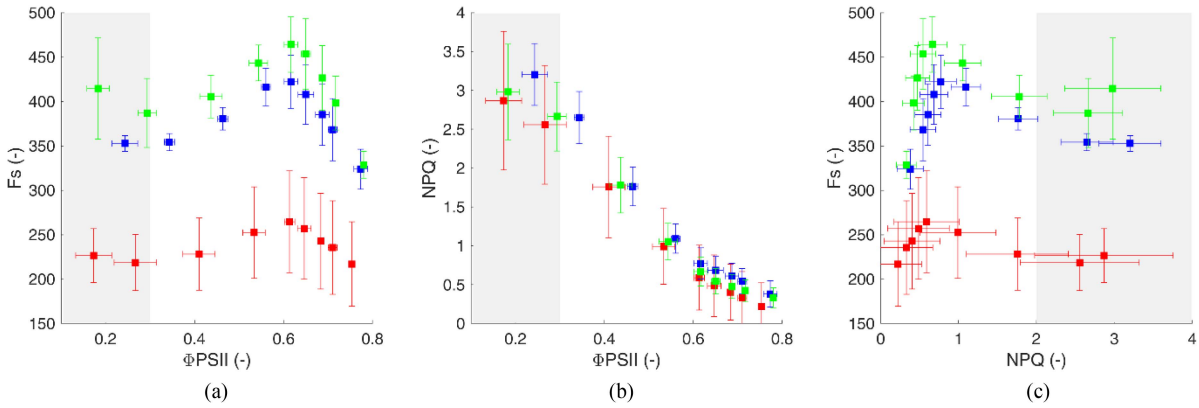

Fig. 4. Light curves measurements, correlation analysis of (a) stable fluorescence (F_s) and quantum yield of photochemical energy conversion (ΦPSII), (b) Non-photochemical quenching (NPQ) and ΦPSII, (c) F_s and NPQ for high nitrogen (green), medium nitrogen (blue), and low nitrogen conditions (red). Conditions in the chamber of the photosynthesis system were reference CO_2 concentration = 400 μmol mol^{-1}, photosynthetically active radiation (PAR) = 0–1800 μmol m^{-2} s^{-1} and leaf temperature set to ambient temperature. The light curve measurements were performed in the middle of the season. The gray shadow areas indicate the ΦPSII range obtained during the seasonal measurements (see Fig. 3) and the corresponding F_s and NPQ values. Number of replicates, $n = 3$ per nitrogen treatment. Error bars represent standard deviation within replicates for each day and treatment.

(0.40–0.50) of ΦPSII. Regarding NPQ and ΦPSII, a consistent negative correlation was observed [see Fig. 4(b)], indicating that low photosynthetic activity is associated with increases in NPQ and vice versa. Contrasting patterns were observed when comparing the relationship between F_s and NPQ. A positive correlation was noted for low (0–1) and high (3–4) values of NPQ, while an inverse relationship was observed for intermediate values (1–3) of NPQ [see Fig. 4(c)]. In Fig. 4, the gray shaded area represents the range of ΦPSII obtained during the seasonal measurements [see Fig. 2(i)] and the corresponding values of fluorescence (F_s) and NPQ for the same range of ΦPSII. From the areas highlighted in gray, and in agreement with Fig. 3(j), it can be observed that during the experiment, the relationship between fluorescence and ΦPSII was slightly negative [see Fig. 4(a)], and that NPQ was highly activated, reaching its saturation phase. This is evidenced by the slight increases in NPQ at low ΦPSII and the ascending trend of F_s at high NPQ values [see Fig. 4(b) and (c)]. Moreover, although comparable trends were identified across the three nitrogen treatments, the magnitude of the observed effects differed between treatments. In this regard, the LN treatment showed lower values than the MN and HN treatments.

Finally, a comparative analysis of the effects of LN, MN, and HN on total dry weight biomass, A_{net}, APAR-Chla, $\hat{A}eff_{max}Chla$, NDVI, RedEdge index, NAOC, ΦPSII, FQE, APAR-CarbXan, and PRI for all measurement days, BS, MD, and ES was conducted (see Table I). Comparable statistical results were observed between dry weight biomass and A_{net}. When all measurement days were considered, statistically significant differences were observed between the LN, MN, and HN treatments for the NDVI, RedEdge index, NAOC, FQE, and PRI (p-value < 0.05, Table I). However, no statistically significant differences were found for total dry biomass, A_{net}, $\hat{A}eff_{max}Chla$, ΦPSII, and APAR-CarbXan. For most parameters and seasonal stages considered in this study, no statistically significant differences were observed between MN and HN. For the MS, none of the studied parameters were able to differentiate between these two treatments. However, during the BS and ES period, NDVI, RedEdge, NAOC, and PRI were able to differentiate between the three nitrogen treatments (p-value $<$ 0.05, Table I).

B. Modeling Net Photosynthesis

Overall the linear LUE models performed a poor seasonal estimation of A_{net}. The LUE-MM and LUE-RSM performed worst with a R^2 = 0.02–0.37 and variance of 4–9 μmol CO_2 m^{-2} s^{-1} of a maximum of 30 μmol CO_2 m^{-2} s^{-1} (see Fig. 5 and Tables S1 and S2, Supplementary material). In the case of the LUE-Berry model a notable improvement in the estimation of A_{net} was observed with an R^2 of 0.40–0.57 and a variance of 3–6 μmol CO_2 m^{-2} s^{-1} (see Fig. 5 and Tables S1 and S2, Supplementary material).

In order to evaluate the linear LUE models, it is necessary to consider two factors: 1) the parameters selected as proxies for FAPAR and 2) the parameters used as proxies for LUE. The linear correlation between each of the parameters used as proxies for FAPAR (i.e., NDVI, RedEdge index, NAOC, and $\hat{A}eff_{max}Chla$) and FAPAR-fluowat was evaluated for the various data set combinations (i.e., All, BS, MS, ES, LN, MN, HN) (see Fig. S3). A positive and statistically significant linear relationship was observed between all FAPAR proxies and FAPAR-fluowat (p-value < 0.05), with the RedEdge and NAOC indices providing the most optimal results (R^2 = 0.66–0.89). This indicates that the parameter used as a FAPAR proxy was not the limiting factor in the model performance. The sum of $\hat{A}eff_{max}Chla$, $\hat{A}eff_{max}Chlb$, $\hat{A}eff_{max}Xan$, and $\hat{A}eff_{max}Carb$ (collectively, $\hat{A}eff_{max}Pigments$) was also evaluated in comparison to FAPAR-fluowat. The use of $\hat{A}eff_{max}Pigments$ as a proxy for FAPAR resulted in a higher linear correlation with FAPAR-fluowat in comparison to $\hat{A}eff_{max}Chla$ (R^2 increased by 30%). However, this did not lead to better results than RedEdge and NAOC. The $\hat{A}eff_{max}Pigments$ was excluded from subsequent analysis and models for two reasons. First, it did not offer any additional insights beyond those provided by RedEdge and NAOC. Second, we sought to assess the potential contribution of the various pigment fractions of absorbed PAR in nonlinear models.

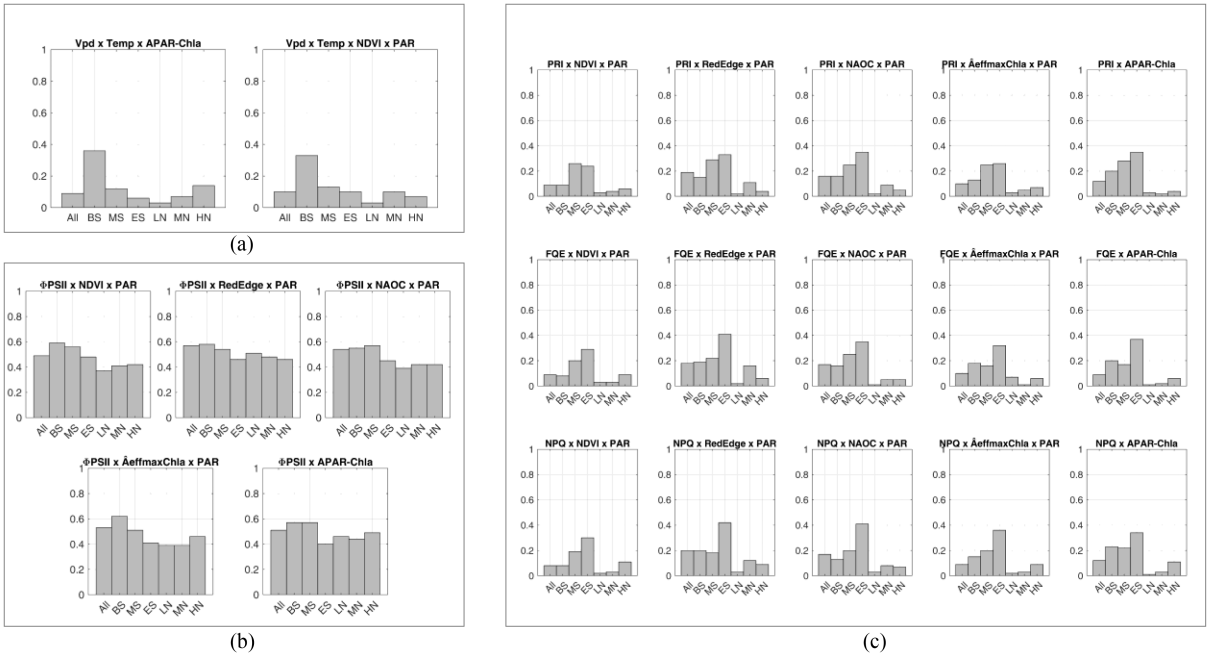

Fig. 5. Coefficient of correlation (R^2) between the measured A_{net} and the modeled A_{net} based on (a) meteorological-driven methods (LUE-MM), (b) Berry-based methods (LUE-Berry), and (c) remote sensing-based methods (LUE-RSM). The models were evaluated based on the complete data set (All), considering only the data collected at beginning of the session (BS), middle of the season (MS), and end of the season (ES), as well as the effect of treatment low nitrogen (LN), middle nitrogen (MN), and high nitrogen (HN) on the seasonal dynamics of photosynthesis. The data available was randomly split into half-sets: 50% samples for training and 50% samples for testing performance. Each model was repeated 10 times, and the average results are provided in the supplementary material Tables S1–S3.

Regarding the parameters used as proxies for LUE, these include Tair and Vpd in LUE-MM models and PRI, FQE, and APAR-CarbXan in LUE-RSM models. No clear pattern was observed with respect to which proxy of LUE improved the performance of the model [see Fig. 5(a) and (c) and Tables S1 and S2, Supplementary material]. In contrast, the LUE-Berry model, in which ΦPSII was taken as a proxy for LUE, resulted in a substantial improvement in the estimation of A_{net} model [see Fig. 5(b) and Table S3, Supplementary material]. The seasonal patterns previously described (see Fig. 3) and the linear correlation between LUE (LUE $= A_{net}$/APAR-Chla) and V_{pd}, T_{air}, ΦPSII, FQE, and PRI corroborate the model results. No univocal relationship was identified between the pair of parameters (see Fig. 6). Only ΦPSII demonstrated a significant positive linear relationship with LUE across seasons and nitrogen treatments [see Fig. 6(c), $R^2 = 0.20$–0.53, p-value < 0.05]. Consequently, the findings are inconclusive regarding the question of whether one LUE proxy is preferable to another in terms of enhancing model predictions for the linear LUE models, with the exception of ΦPSII. However, this cannot be estimated remotely.

Based on the average linear models results, a set of nonlinear LUE models were constructed using the Gaussian process regression (GPR) method, which enabled the estimation of the amount of information about A_{net} that could be derived from a nonlinear combination of the measured variable. The GPR models were constructed in a series of steps. Initially, a more basic approach was utilized, whereby only a single parameter was considered. This was subsequently developed into a more complex model, in which a maximum of six parameters are combined to estimate A_{net}. A total of 308 models were tested for each data set (i.e., all data, BS, MN, ES, LN, MN, and HN), resulting in a total of 2156 simulations (308 x 7 dataset). In consideration of the extension of the results, this manuscript presents a summary of the most relevant results (see Fig. 7 and Tables S4 and S5, Supplementary material). Additionally, a spreadsheet is provided as Supplementary material, wherein the outcomes of each model iteration are shown (Supplementary material spreadsheet GPR models results). The main findings will be presented as a range of percentages representing the observed variability for each parameter or combination of parameters. The described range includes all data sets that were subjected to testing (i.e., all data, BS, MN, ES, LN, MN, and HN).

As excepted from previous results when only one parameter was considered, approximately 36%–50% of A_{net} variability was explained by ΦPSII with a variance of 3–6 μmol CO_2 m^{-2} s^{-1}, followed by the RedEdge index (8%–40%—variance 4–7 μmol CO_2 m^{-2} s^{-1}), and V_{pd} and/or T_{air} (2%–30%—variance 4–7 μmol CO_2 m^{-2} s^{-1}). FQE and APAR-CarbXan were found to account for only 2%–5% of A_{net} variability when considered independently (supplementary material spreadsheet GPR models results). When two parameters were considered, the best results were obtained when A_{net} was modeled as a function of ΦPSII together with a chlorophyll content-related VI (i.e., RedEdge). This model explained between 42% and 58% of the A_{net} variability with variance ~ 4 μmol CO_2 m^{-2} s^{-1} (Supplementary material spreadsheet GPR models results). When the model was defined by Vpd and Tair, it explained between 38% and 67% of the variability (ES) [see Fig. 7(a)]. Regarding FQE and APAR-CarbXan, when they were paired with a chlorophyll content-related VI (i.e., RedEdge), they explained between 1% and 45% of A_{net} variability (Supplementary material spreadsheet GPR models results). In all cases, the poorest results were

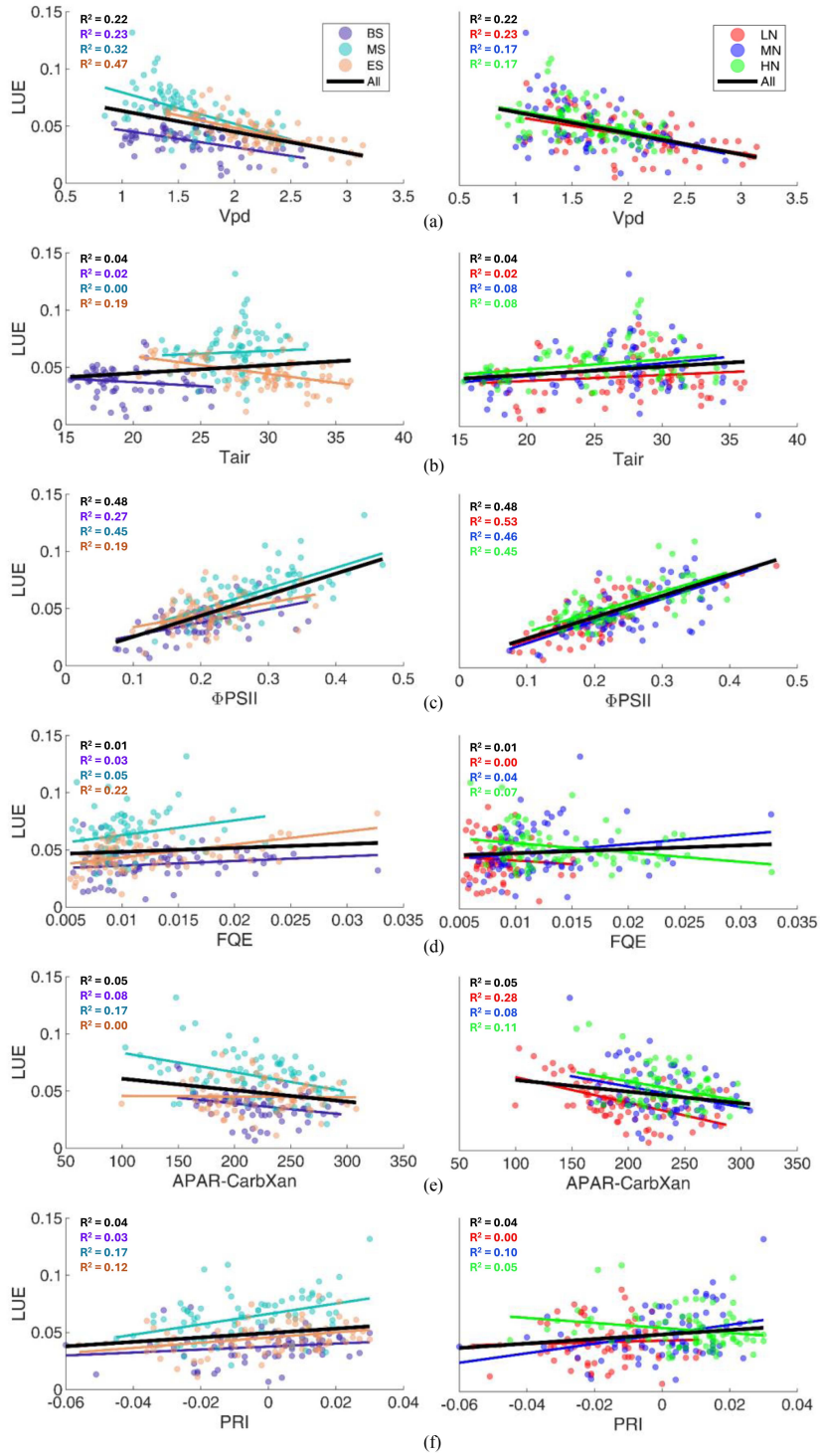

Fig. 6. Linear correlation and coefficient of correlation (R^2) between seasonal periods (left plots) and within treatments (right plots) for light use efficiency (LUE $= A_{\rm net}$/APAR-Chla, -) and (a) vapor pressure deficit ($V_{\rm pd}$, *K*Pas), (b) air temperature (Tair, Celsius), (c) quantum yield of photochemical energy conversion (ΦPSII, -), (d) fluorescence quantum yield (FQE, -), (e) photon flux absorbed by beta-Carotene and xanthophyll pigments (APAR-CarbXan, μmol m^{-2} s^{-1}), and (f) the Photochemical Reflectance Index (PRI, -) in wheat plants grown under low (LN), medium (MN), and high nitrogen (HN) conditions. The three seasonal periods described in the manuscript are the beginning of the season (days after sowing (DAS) 77 to 91, BS), the middle of the season (DAS 105 to 119, MS), and the end of the season (DAS 126 to 140, ES). This aligns with the wheat growth stages of jointing (BS), heading and anthesis (MS), and grain filling (ES).

obtained when only the LN data set was considered, whereas the most favorable outcomes were obtained when All, BS, MS, ES, and HN datasets were considered [see Fig. 7(a)–(c), and Supplementary material spreadsheet GPR models results].

The construction of the model based on three or more parameters led to the best results when ΦPSII was combined with chlorophyll content-related variable (i.e., RedEdge), PAR, $V_{\rm pd}$, and $T_{\rm air}$, explaining 63%–73% of $A_{\rm net}$ variability with variance

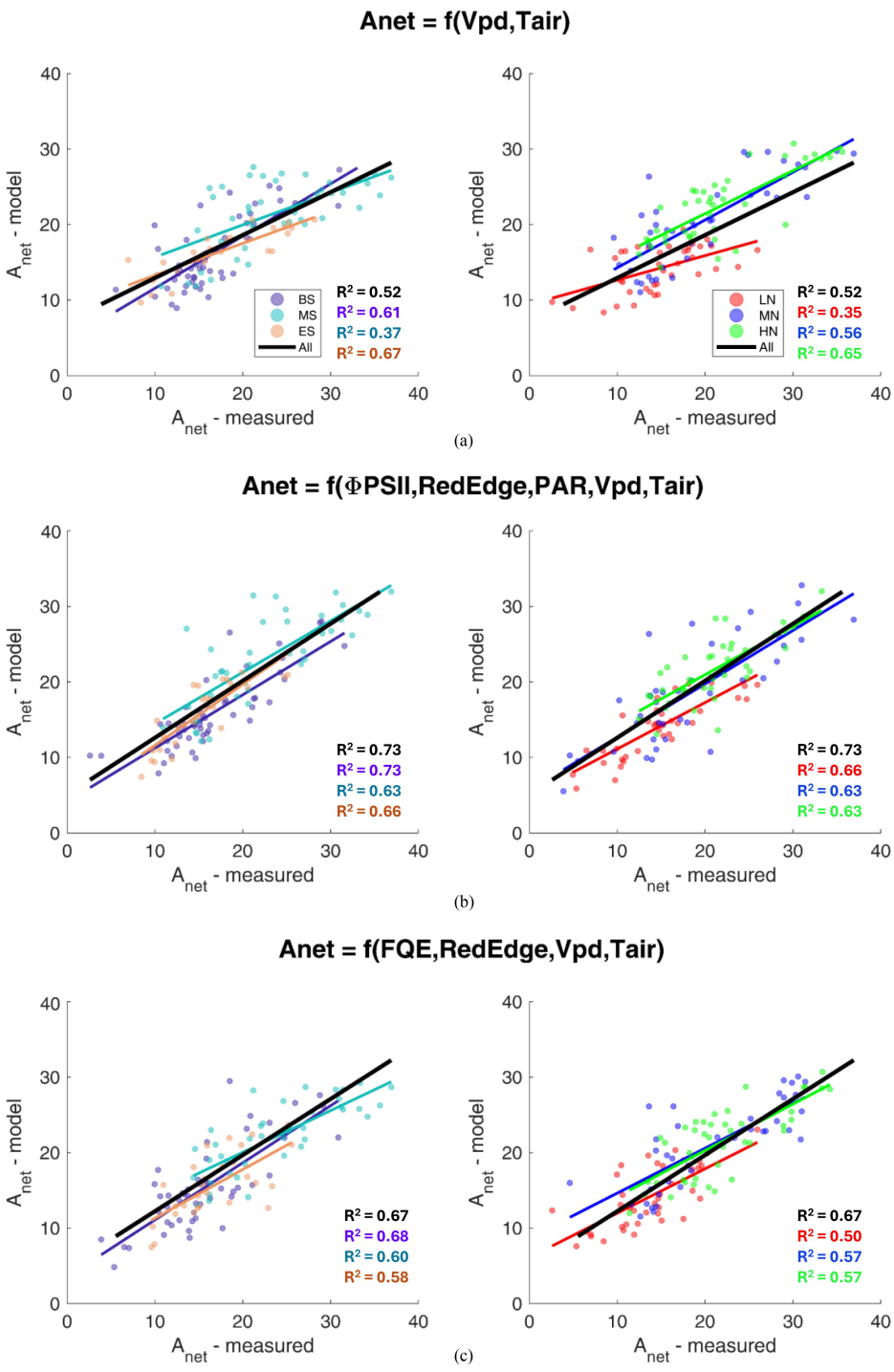

Fig. 7. Linear correlation and coefficient of correlation (R^2) between seasonal periods (left plots) and within treatments (right plots) for the measured net photosynthesis (A_{net}—measured) and the modeled net photosynthesis (A_{net}—modeled) for the best-performing models when (a) only two parameters were considered, (b) the quantum yield of photochemical energy conversion (ΦPSII), was included through the process of model definition, and (C) when ΦPSII was not included through the process of model definition in wheat plants grown under low (LN), medium (MN), and high nitrogen (HN) conditions. The three seasonal periods described in the manuscript are the beginning of the season (days after sowing (DAS) 77 to 91, BS), the middle of the season (DAS 105 to 119, MS), and the end of the season (DAS 126 to 140, ES). This aligns with the wheat growth stages of jointing (BS), heading and anthesis (MS), and grain filling (ES). The data available was randomly split into half-sets: 50% samples for training and 50% samples for testing performance. Each model was repeated 10 times, and the average results are provided in the supplementary material spreadsheet GPR models results and Table S4-S5. The rankings are based on the best results for R^2 and AIC.

$\sim$ 4 μmol CO_2 m^{-2} s^{-1} [see Figs. 7(b), 8(a), and Table S4]. As ΦPSII, cannot be directly measured using remote sensing techniques, the performance of the models in which it is not included was also evaluated. The combination of primarily FQE and secondly PRI or APAR-CarbXan with chlorophyll content-related VI (i.e., RedEdge), PAR, VPD, and Tair explained approximately 47-69% of the variability with variance $\sim$ 4 μmol CO_2 m^{-2} s^{-1} [see Figs. 7(c), 8(b), and Table S5,

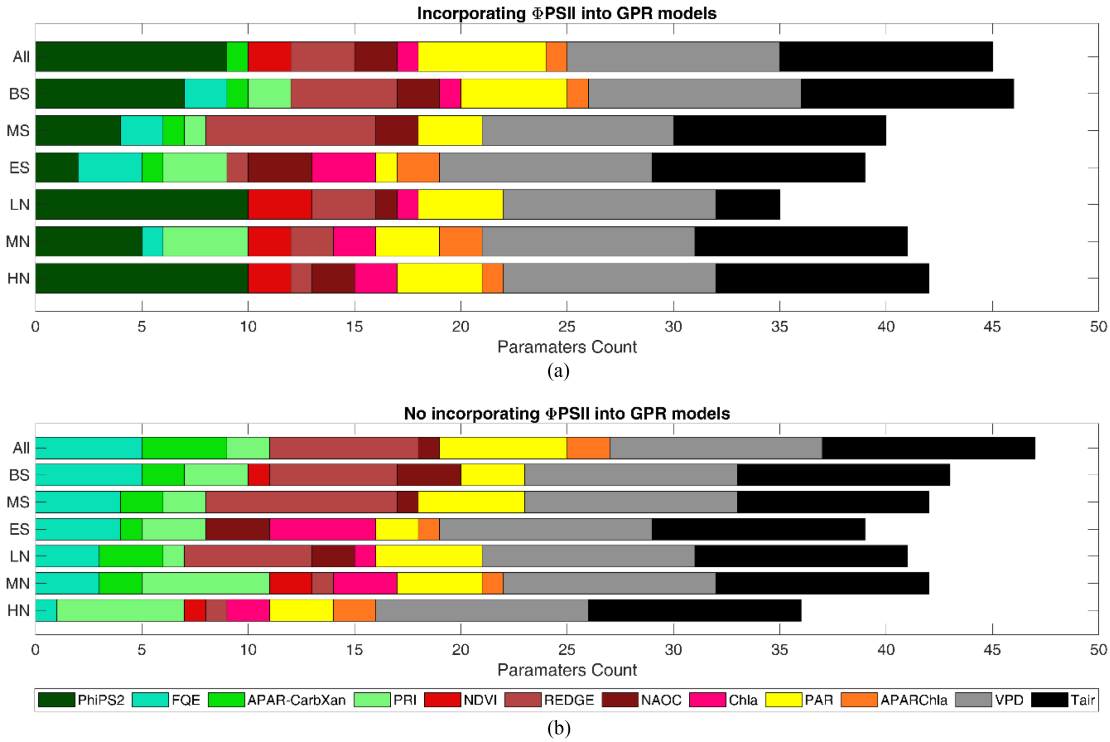

Fig. 8. Summary of the parameters that are most frequently incorporated into the ten best-performing Gaussian process regression (GPR) method models. (a) Quantum yield of photochemical energy conversion (ΦPSII), was included through the process of model definition, and (b) when ΦPSII was not included through the process of model definition in wheat plants grown under low (LN), medium (MN), and high nitrogen (HN) conditions. The three seasonal periods described in the manuscript are the beginning of the season (days after sowing (DAS) 77 to 91, BS), the middle of the season (DAS 105 to 119, MS), and the end of the season (DAS 126 to 140, ES). A complete overview of the results obtained by each model are provided in the supplementary material spreadsheet GPR models results and Table S4-S5.

Supplementary material]. The Supplementary material presents a comprehensive overview of all model combinations, including the ten most optimal models, both with and without the consideration of ΦPSII. These are provided in Tables S4 and S5, Supplementary material, respectively. Furthermore, Fig. 8 presents a summary of the parameters that are most frequently repeated in the best-performing models. In the case of a model incorporating ΦPSII, these are ΦPSII, RedEdge index, PAR, V_{pd}, and T_{air}. Additionally, when ΦPSII was not considered, FQE followed by PRI and APAR-CarbXan were more predominant in the best-performing models.

IV. Discussion

The observed seasonal trends in photosynthetic parameters and biophysical traits are closely related to the phenological stages of wheat. During the early growth stages (BS and MS), plants were actively growing and developing. The increased nitrogen availability in the MN and HN treatments probably stimulated rapid growth, resulting in higher leaf area (data not shown), chlorophyll content, and photosynthetic capacity. This is reflected in the increased values of A_{net}, LUE, and ΦPSII during these stages. As the crop matured (ES), increased resource allocation to grain filling and maturation likely diverted energy away from leaf growth and photosynthesis. This could explain the decrease in A_{net}, LUE and ΦPSII during this later stage. Among the indices used as a proxy for FAPAR, only the RedEdge index effectively captured the described seasonal variability. This index is sensitive to changes in the red absorption tail of chlorophyll in the 680–750 nm range, making it more sensitive to changes in chlorophyll concentration [57]. For NDVI and NAOC we hypothesize that their saturation at high nitrogen concentrations may limit their ability to capture the full extent of seasonal variability [58]. In addition, the $\hat{A}\mathrm{eff}_{\mathrm{max}}\mathrm{Chla}$ fitting algorithm may require refinement to better account for seasonal changes in chlorophyll content. Finally, for MN and HN, FQE, APAR-CarbXan and PRI showed opposite trends to A_{net}, LUE and ΦPSII, highlighting the dynamic interplay between these parameters. This suggests that incorporating nonlinear relationships between photosynthesis and these parameters into photosynthesis models could improve their predictive capabilities.

In the case of LUE-based models, the seasonal variability of photosynthesis can be explained by three key variables: FAPAR, LUE, and a correction factor related to meteorological conditions that limit LUE [21], [22]. Overall changes in FAPAR are regulated by leaf pigment concentration and chlorophyll absorption behavior, where the red edge region has been also shown susceptible to changes when NPQ is activated [3], [59], [60]. The red edge is mainly sensitive to changes in chlorophyll content, as an increase in chlorophyll concentration broadens the absorption features and moves the red edge to longer wavelengths [61]. This is expected to be the main reason why the RedEdge and NAOC indices were highly correlated with the total FAPAR-fluowat in this study (R^2>0.70, p-value $<$ 0.05, Fig. S4). Regarding

LUE, where A_{net}/APAR-Chla was used as a proxy, neither Vpd, Tair, FQE, APAR-CarbXan nor PRI presented a similar trend and did not show a strong correlation with LUE [$R^2 < 0.33$, except Vpd-ES with a $R^2 = 0.47$, Figs. 2(b)–(c), 3(j)–(l), and Fig. 6(a)–(b) and (d)–(f)]. In contrast, ΦPSII showed a seasonal trend similar to LUE and A_{net} [see Fig. 3(a) and (b)], with a coefficient of correlation between seasonal periods and within treatments ranging from 0.19 (ES) to 0.53 (LN) [p-value $<$ 0.05, Fig. 6(c)]. An interesting result of this study is that ΦPSII observations fluctuated between 0.10–0.40, however unstressed leaves are characterized by having ΦPSII values close to 0.8 which correlates with the maximum yield of photosynthesis in the light adapted state [62]. Therefore, the observed ΦPSII values indicated a strong downregulation of the photosystem II machinery during the measurement period. We hypothesized that the high growing illumination conditions to which plants were exposed [i.e., 1500–1900 mmol m^{-2} s^{-1}, Fig. 3(a) and (b)] were the cause of the photosynthetic downregulation. Similar ΦPSII results (0.1–0.4) were observed at the ΦPSII versus PAR curves when illumination conditions reached values higher than 700 mmol m^{-2} s^{-1} (data not shown).

The trends just described are consistent with the results obtained when modeling A_{net} by the meteorology (MM), remote-sensing (RSM), and Berry LUE linear-based methods. No FQE, APAR-CarbXan, and PRI nor the linear combination of these parameters were able to model the seasonal changes of A_{net} (see Fig. 5, Tables S1–S3). We hypothesized that the primary limitation of linear models in this context lies in their inherent focus on long-term trends in canopy greenness and environmental conditions [63]. While these models are well-suited for capturing broad-scale variations, they may struggle to accurately represent the more nuanced, short-term fluctuations observed in leaf-level measurements. These rapid changes, influenced by factors such as light intensity, temperature, and humidity, can introduce nonlinear relationships that linear models are ill-equipped to capture. In contrast to previous studies [27], [33], [34], no positive linear relationship was observed between fluorescence (i.e., FQE) and LUE [see Fig. 6(d)]. This divergence likely stems from the high NPQ activation under stress conditions of our experiment (ΦPSII = 0.10–0.40, shaded area in Fig. 4). Under this conditions, NPQ mechanisms control the energy dissipation pathway, thus disrupting the expected linear relationship (Fig. 4, F_s-vs-ΦPSII and NPQ-vs-ΦPSII light curves) [36], [38], [64]. Satellite platforms, which are limited to passive measurements, cannot directly measure ΦPSII, which prevents the direct application of the Berry-based model. Our study corroborates that leaf-scale ΦPSII measurements can provide insight into the mechanisms controlling SIF and NPQ, ultimately contributing to the development of more robust models for estimating photosynthesis (see Figs. 3 and 4). This aligns with the ESA Fluorescence Explore (FLEX) mission's goal of deriving a photosynthetic efficiency proxy from satellite-derived SIF and NPQ data, enabling remote estimation of photosynthesis rates and early stress detection [65].

Our study showed that, in both cases between seasonal periods and within treatments, A_{net} changes could be more accurately explained when LUE and APAR proxies together with meteorological conditions were combined in a nonlinear model. For example, in the case of the LUE-MM linear model [see Fig. 5(a) and Table S1, Supplementary material], where NDVI or APAR-Chla were combined with V_{pd} and T_{air} to model A_{net}, the coefficient of determination ranged between 0.07 and 0.36. However, when V_{pd} and T_{air} (dark reaction proxies, Fig. 1) were combined using a nonlinear model, the R^2 increased up to 0.35–0.67 [see Fig. 7(a) and Table S4]. Furthermore, when V_{pd} and T_{air} were combined with APAR (i.e., RedEdge and PAR) and light reaction (i.e., ΦPSII or FQE) proxies, the coefficient of determination increased, reaching values of 0.63–0.73 for ΦPSII and 0.50–0.68 for FQE (Supplementary material spreadsheet and Fig. 7). Most of the models considered performed better when the complete dataset (All) and the seasonal period (BS, ES, MS) were included than when only the within-treatment dataset was used (see Fig. 7 and Tables S1–S5, Supplementary material). For the complete dataset and between seasonal periods, the different nitrogen treatments are considered together. Thus, the nitrogen content gradient (see Table I) serves as the primary driver of seasonal patterns in leaf chlorophyll content and APAR, thereby improving the model performance. In contrast, when only within-treatment data were considered, in this study, the weakest seasonal variation within a treatment resulted in the poorest model performance (see Fig. 7 and Tables S1–S5, Supplementary material).

In this study, APAR-CarbXan and PRI (i.e., NPQ proxies) tracked the long-term (weeks) variations driven by the carotenoid/chlorophyll ratio [66], [67], which for low values of ΦPSII reaches saturation and does not show pronounced changes between treatments [see Fig. 4(b) and (c)] and over the course of the season (see Fig. 3). For this reason, APAR-CarbXan and PRI did not contribute significantly to the A_{net} predictions in this study.

To summary, in this study, chlorophyll content controlled the fraction of photosynthetically active radiation absorbed by the leaf (FAPAR, Fig. S3, Supplementary material); ΦPSII and FQE provided an estimate of the actual photochemical quenching efficiency of the light reaction [43], [68]; and V_{pd}, together with T_{air}, controlled stomatal opening (CO_2 uptake) and thus the biochemical reactions involved in the conversion of absorbed energy into sugars and carbon assimilation during the dark reactions of photosynthesis (see Fig. 1) [69]. ΦPSII, which is positively correlated with LUE [see Figs. 3(i) and 6], cannot be measured remotely. However, FQE, which in this experiment showed an opposite trend to LUE [see Fig. 3(b) and (j)] and a negative linear correlation with ΦPSII [see Fig. 4(a), grey shadow area], can be derived from reflected radiance measurements. The application of FQE in a linear model did not result in improved model performance. However, the incorporation of a non-linear relationship between LUE and FQE in combination with the RedEdge index, V_{pd} and T_{air}, through the use of the GPR method, led to improvements in model performance (see Tables S2–S5, Supplementary material, and Fig. 7). This study confirms the need to develop nonlinear models for a proper implementation of SIF in global photosynthesis models [36], [70]. Nevertheless, the results presented here are based on a limited data set in which the NPQ mechanism is strongly activated,

facing saturation. To develop a robust nonlinear model, it is necessary to have a complete dataset that includes information on the different SIF versus ΦPSII and NPQ versus ΦPSII phases across a variety of species and climatic zones.

Furthermore, additional work is required to extrapolate these results to the canopy level, where canopy structure plays a significant role in the optimization and regulation of plant photosynthesis. In this study, both FQE and APAR-CarbXan were retrieved based on a bottom-up approach, wherein a spectral unmixing technique was employed to estimate the effective absorbance of individual pigments, with the objective of establishing a link between the true molecular chlorophyll fluorescence and the apparent fluorescence emission [28]. Nevertheless, in future studies, in order to recover fluorescence emission at the molecular level, it is mandatory to consider the effects of leaf and canopy scattering and reabsorption, as well as the PSI-PSII contribution to total fluorescence emission [65], [71].

V. Conclusion

The objective of this study was to assess seasonal trends and relationships observed between photosynthesis, structural, and physiological optical indices, and chlorophyll fluorescence at the leaf level in a well-watered wheat field growing under different nitrogen treatments. Our findings corroborate the hypothesis that, under stress conditions, incorporating a nonlinear relationship between LUE and FQE led to improvements in model performance. This reinforces the necessity for more complex, nonlinear models to disentangle the contribution of light and dark reactions to carbon assimilation processes. This study emphasized the necessity for seasonal measurements (at the leaf, plant, and field levels) of chlorophyll fluorescence, along with other biophysical parameters (such as chlorophyll content and thermal dissipation), to provide a comprehensive understanding of their contributions to the dynamic regulation of the light reactions under diverse plant conditions and stress scenarios.

Acknowledgment

The authors are grateful to Susan Moran, Marina Martinez-Garcia, Micol Rossini, Kelly Thorp, and Guangyao Wang for their expert advice. The authors also thank the reviewers for their thorough review and constructive feedback, which improved the clarity and understanding of this manuscript. Raw and processed data are available open access through the Zenodo repository (doi: 10.5281/zenodo.15227508).

References

[1] E. H. Murchie, M. Pinto, and P. Horton, "Agriculture and the new challenges for photosynthesis research," *New Phytologist*, vol. 181, no. 3, pp. 532–552, Feb. 2009, doi: 10.1111/j.1469-8137.2008.02705.x.

[2] S. Liang and J. Wang, Eds., "Chapter 15 - estimate of vegetation production of terrestrial ecosystem," in *Advanced Remote Sensing*, 2nd ed. New York, NY, USA: Academic, 2020, pp. 581–620, doi: 10.1016/B978-0-12-815826-5.00015-5.

[3] S. Van Wittenberghe, L. Alonso, Z. Malenovský, and J. Moreno, "In vivo photoprotection mechanisms observed from leaf spectral absorbance changes showing VIS–NIR slow-induced conformational pigment bed changes," *Photosynthesis Res.*, vol. 142, no. 3, pp. 283–305, Dec. 2019, doi: 10.1007/s11120-019-00664-3.

[4] S. Van Wittenberghe, V. Laparra, J. I. García-Plazaola, B. Fernández-Marín, A. Porcar-Castell, and J. Moreno, "Combined dynamics of the 500–600 nm leaf absorption and chlorophyll fluorescence changes in vivo: Evidence for the multifunctional energy quenching role of xanthophylls," *Biochimica et Biophysica Acta, Bioenergetics*, vol. 1862, no. 2, Feb. 2021, Art. no. 148351, doi: 10.1016/j.bbabio.2020.148351.

[5] M. Meroni et al., "Remote sensing of solar-induced chlorophyll fluorescence: Review of methods and applications," *Remote Sens. Environ.*, vol. 113, no. 10, pp. 2037–2051, Oct. 2009, doi: 10.1016/j.rse.2009.05.003.

[6] G. H. Mohammed et al., "Remote sensing of solar-induced chlorophyll fluorescence (SIF) in vegetation: 50 years of progress," *Remote Sens. Environ.*, vol. 231, Sep. 2019, Art. no. 111177, doi: 10.1016/j.rse.2019.04.030.

[7] A. Porcar-Castell, "A high-resolution portrait of the annual dynamics of photochemical and non-photochemical quenching in needles of Pinus sylvestris," *Physiologia Plantarum*, vol. 143, no. 2, pp. 139–153, 2011, doi: 10.1111/j.1399-3054.2011.01488.x.

[8] N. Betterle et al., "Light-induced dissociation of an antenna hetero-oligomer is needed for non-photochemical quenching induction," *J. Biol. Chem.*, vol. 284, no. 22, pp. 15255–15266, May 2009, doi: 10.1074/jbc.M808625200.

[9] L. Dall'Osto, S. Caffarri, and R. Bassi, "A mechanism of nonphotochemical energy dissipation, independent from PsbS, revealed by a conformational change in the antenna protein CP26," *Plant Cell*, vol. 17, no. 4, pp. 1217–1232, Apr. 2005, doi: 10.1105/tpc.104.030601.

[10] S. de Bianchi, M. Ballottari, L. Dall'osto, and R. Bassi, "Regulation of plant light harvesting by thermal dissipation of excess energy," *Biochem. Soc. Trans.*, vol. 38, no. 2, pp. 651–660, Apr. 2010, doi: 10.1042/BST0380651.

[11] M. Havaux and K. K. Niyogi, "The violaxanthin cycle protects plants from photooxidative damage by more than one mechanism," *Proc. Nat. Acad. Sci.*, vol. 96, no. 15, pp. 8762–8767, Jul. 1999, doi: 10.1073/pnas.96.15.8762.

[12] A. R. Holzwarth, Y. Miloslavina, M. Nilkens, and P. Jahns, "Identification of two quenching sites active in the regulation of photosynthetic light-harvesting studied by time-resolved fluorescence," *Chem. Phys. Lett.*, vol. 483, no. 4, pp. 262–267, Dec. 2009, doi: 10.1016/j.cplett.2009.10.085.

[13] P. Horton and A. Ruban, "Molecular design of the photosystem II light-harvesting antenna: Photosynthesis and photoprotection," *J. Exp. Botany*, vol. 56, no. 411, pp. 365–373, Jan. 2005, doi: 10.1093/jxb/eri023.

[14] L. Kalituho, K. C. Beran, and P. Jahns, "The transiently generated non-photochemical quenching of excitation energy in arabidopsis leaves is modulated by zeaxanthin," *Plant Physiol.*, vol. 143, no. 4, pp. 1861–1870, Apr. 2007, doi: 10.1104/pp.107.095562.

[15] P. H. Lambrev, Y. Miloslavina, P. Jahns, and A. R. Holzwarth, "On the relationship between non-photochemical quenching and photoprotection of photosystem II," *Biochimica et Biophysica Acta, Bioenergetics*, vol. 1817, no. 5, pp. 760–769, May 2012, doi: 10.1016/j.bbabio.2012.02.002.

[16] M. Nilkens et al., "Identification of a slowly inducible zeaxanthin-dependent component of non-photochemical quenching of chlorophyll fluorescence generated under steady-state conditions in *Arabidopsis*," *Biochimica et Biophysica Acta, Bioenergetics*, vol. 1797, no. 4, pp. 466–475, Apr. 2010, doi: 10.1016/j.bbabio.2010.01.001.

[17] A. V. Ruban, "Plants in light," *Commun. Integr. Biol.*, vol. 2, no. 1, pp. 50–55, Jan. 2009, doi: 10.4161/cib.2.1.7504.

[18] A. V. Ruban, "Nonphotochemical chlorophyll fluorescence quenching: Mechanism and effectiveness in protecting plants from photodamage," *Plant Physiol.*, vol. 170, no. 4, pp. 1903–1916, Apr. 2016, doi: 10.1104/pp.15.01935.

[19] C. Jiang and Y. Ryu, "Multi-scale evaluation of global gross primary productivity and evapotranspiration products derived from breathing earth system simulator (BESS)," *Remote Sens. Environ.*, vol. 186, pp. 528–547, Dec. 2016, doi: 10.1016/j.rse.2016.08.030.

[20] M. Jung et al., "Recent decline in the global land evapotranspiration trend due to limited moisture supply," *Nature*, vol. 467, Oct. 2010, Art. no. 7318, doi: 10.1038/nature09396.

[21] J. L. Monteith, "Solar-radiation and productivity in tropical ecosystems," *J. Appl. Ecol.*, vol. 9, pp. 747–766, 1972.

[22] J. L. Monteith and C. J. Moss, "Climate and the efficiency of crop production in Britain [and discussion]," *Philos. Trans. Roy. Soc. London. Ser. B, Biol. Sci.*, vol. 281, no. 980, pp. 277–294, Nov. 1977, doi: 10.1098/rstb.1977.0140.

[23] D. Kováč, A. Ač, L. Šigut, J. Peñuelas, J. Grace, and O. Urban, "Combining NDVI, PRI and the quantum yield of solar-induced fluorescence improves estimations of carbon fluxes in deciduous and evergreen forests," *Sci. Total Environ.*, vol. 829, Jul. 2022, Art. no. 154681, doi: 10.1016/j.scitotenv.2022.154681.

[24] M. Rossini et al., "Red and far red Sun-induced chlorophyll fluorescence as a measure of plant photosynthesis," *Geophys. Res. Lett.*, vol. 42, no. 6, Mar. 2015, Art. no. 2014GL062943, doi: 10.1002/2014GL062943.

[25] A. Schickling et al., "Combining sun-induced chlorophyll fluorescence and photochemical reflectance index improves diurnal modeling of gross primary productivity," *Remote Sens.*, vol. 8, no. 7, Jul. 2016, Art. no. 574, doi: 10.3390/rs8070574.

[26] G. G. Drolet et al., "A MODIS-derived photochemical reflectance index to detect inter-annual variations in the photosynthetic light-use efficiency of a boreal deciduous forest," *Remote Sens. Environ.*, vol. 98, no. 2, pp. 212–224, Oct. 2005, doi: 10.1016/j.rse.2005.07.006.

[27] X. Yang et al., "Solar-induced chlorophyll fluorescence that correlates with canopy photosynthesis on diurnal and seasonal scales in a temperate deciduous forest," *Geophys. Res. Lett.*, vol. 42, no. 8, pp. 2977–2987, 2015, doi: 10.1002/2015GL063201.

[28] S. Van Wittenberghe et al., "Retrieval of leaf-level fluorescence quantum efficiency and NPQ-related xanthophyll absorption through spectral unmixing strategies for future VIS-NIR imaging spectroscopy," *Remote Sens. Environ.*, vol. 300, Jan. 2024, Art. no. 113879, doi: 10.1016/j.rse.2023.113879.

[29] J. A. Gamon, J. Peñuelas, and C. B. Field, "A narrow-waveband spectral index that tracks diurnal changes in photosynthetic efficiency," *Remote Sens. Environ.*, vol. 41, no. 1, pp. 35–44, Jul. 1992, doi: 10.1016/0034-4257(92)90059-S.

[30] S. Pescador-Dionisio et al., "In vivo detection of spectral reflectance changes associated with regulated heat dissipation mechanisms complements fluorescence quantum efficiency in early stress diagnosis," *New Phytologist*, vol. 245, pp. 559–576, Jan. 2025, doi: 10.1111/nph.20253.

[31] A. Porcar-Castell et al., "Physiology of the seasonal relationship between the photochemical reflectance index and photosynthetic light use efficiency," *Oecologia*, vol. 170, no. 2, pp. 313–323, Oct. 2012, doi: 10.1007/s00442-012-2317-9.

[32] C. Y. S. Wong and J. A. Gamon, "Three causes of variation in the photochemical reflectance index (PRI) in evergreen conifers," *New Phytologist*, vol. 206, no. 1, pp. 187–195, 2015, doi: 10.1111/nph.13159.

[33] H. Kimm et al., "A physiological signal derived from sun-induced chlorophyll fluorescence quantifies crop physiological response to environmental stresses in the U.S. Corn Belt," *Environ. Res. Lett.*, vol. 16, no. 12, Dec. 2021, Art. no. 124051, doi: 10.1088/1748-9326/ac3b16.

[34] T. S. Magney et al., "Mechanistic evidence for tracking the seasonality of photosynthesis with solar-induced fluorescence," *Proc. Nat. Acad. Sci*, vol. 116, pp. 11640–11645, Jun. 2019, doi: 10.1073/pnas.1900278116.

[35] L. He et al., "From the ground to space: Using solar-induced chlorophyll fluorescence to estimate crop productivity," *Geophys. Res. Lett.*, vol. 47, no. 7, 2020, Art. no. e2020GL087474, doi: 10.1029/2020GL087474.

[36] J. F. Moreno, "Advances in the retrieval and interpretation of solar-induced vegetation chlorophyll fluorescence using passive remote sensing techniques," in *Proc. IEEE Int. Geosci. Remote Sens. Symp.*, Jul. 2021, pp. 1915–1918, doi: 10.1109/IGARSS47720.2021.9554239.

[37] T. S. Magney, M. L. Barnes, and X. Yang, "On the covariation of chlorophyll fluorescence and photosynthesis across scales," *Geophys. Res. Lett.*, vol. 47, no. 23, 2020, Art. no. e2020GL091098, doi: 10.1029/2020GL091098.

[38] D. Martini et al., "Heatwave breaks down the linearity between sun-induced fluorescence and gross primary production," *New Phytologist*, vol. 233, no. 6, pp. 2415–2428, 2022, doi: 10.1111/nph.17920.

[39] A. Porcar-Castell et al., "Linking chlorophyll a fluorescence to photosynthesis for remote sensing applications: mechanisms and challenges," *J. Exp. Bot.*, vol. 65, no. 15, Aug. 2014, pp. 4065–4095, doi: 10.1093/jxb/eru191.

[40] K. R. Thorp, G. Wang, K. F. Bronson, M. Badaruddin, and J. Mon, "Hyperspectral data mining to identify relevant canopy spectral features for estimating durum wheat growth, nitrogen status, and grain yield," *Comput. Electron. Agriculture*, vol. 136, pp. 1–12, Apr. 2017, doi: 10.1016/j.compag.2017.02.024.

[41] E. Carmo-Silva et al., "Phenotyping of field-grown wheat in the U.K. highlights contribution of light response of photosynthesis and flag leaf longevity to grain yield," *J. Exp. Botany*, vol. 68, no. 13, pp. 3473–3486, Aug. 2017, doi: 10.1093/jxb/erx169.

[42] M. P. Cendrero-Mateo et al., "Plant chlorophyll fluorescence: Active and passive measurements at canopy and leaf scales with different nitrogen treatments," *J. Exp. Botany*, vol. 67, no. 1, pp. 275–286, Jan. 2016.

[43] N. R. Baker, "Chlorophyll fluorescence: A probe of photosynthesis in vivo," *Annu. Rev. Plant Biol.*, vol. 59, no. 1, pp. 89–113, 2008, doi: 10.1146/annurev.arplant.59.032607.092759.

[44] L. Alonso and J. Moreno, "A novel portable device to measure leaf reflectance, transmittance, and fluorescence emission under natural conditions," in *Proc. 4rd Int. Workshop Remote Sens. Vegetation Fluorescence*, 2010, doi: 10.13140/RG.2.1.3052.7523.

[45] C. J. Tucker, "Red and photographic infrared linear combinations for monitoring vegetation," *Remote Sens. Environ.*, vol. 8, no. 2, pp. 127–150, May 1979, doi: 10.1016/0034-4257(79)90013-0.

[46] J. E. Vogelmann, B. N. Rock, and D. M. Moss, "Red edge spectral measurements from sugar maple leaves," *Int. J. Remote Sens.*, vol. 14, no. 8, pp. 1563–1575, May 1993, doi: 10.1080/01431169308953986.

[47] P. J. Zarco-Tejada, J. R. Miller, T. L. Noland, G. H. Mohammed, and P. H. Sampson, "Scaling-up and model inversion methods with narrowband optical indices for chlorophyll content estimation in closed forest canopies with hyperspectral data," *IEEE Trans. Geosci. Remote Sens.*, vol. 39, no. 7, pp. 1491–1507, Jul. 2001, doi: 10.1109/36.934080.

[48] J. Delegido, L. Alonso, G. González, and J. Moreno, "Estimating chlorophyll content of crops from hyperspectral data using a normalized area over reflectance curve (NAOC)," *Int. J. Appl. Earth Observation Geoinf.*, vol. 12, no. 3, pp. 165–174, Jun. 2010, doi: 10.1016/j.jag.2010.02.003.

[49] F. A. Heinsch, M. Reeves, and P. Votava, *Users Guide: GPP and NPP (MOD17A2/A3) Products NASA MODIS Land Algorithm*. Missoula, MT, USA: Univ. Montana, 2003.

[50] M. Rossini et al., "High resolution field spectroscopy measurements for estimating gross ecosystem production in a rice field," *Agricultural Forest Meteorol.*, vol. 150, no. 9, pp. 1283–1296, Aug. 2010, doi: 10.1016/j.agrformet.2010.05.011.

[51] A. Berry, C. Frankenbergand, and P. Wennberg, "New methods for measurements of photosynthesis from space," Keck Inst. Space Stud., Pasadena, CA, USA, Apr. 2013. [Online]. Available: https://doi.org/10.26206/9NJP-CG56

[52] G. Camps-Valls, J. Verrelst, J. Munoz-Mari, V. Laparra, F. Mateo-Jimenez, and J. Gomez-Dans, "A survey on Gaussian processes for earth-observation data analysis: A comprehensive investigation," *IEEE Geosci. Remote Sens. Mag.*, vol. 4, no. 2, pp. 58–78, Jun. 2016, doi: 10.1109/MGRS.2015.2510084.

[53] M. Lázaro-Gredilla, M. Titsias, J. Verrelst, and G. Camps-Valls, "Retrieval of biophysical parameters with heteroscedastic Gaussian processes," *IEEE Geosci. Remote Sens. Lett.*, vol. 11, no. 4, pp. 838–842, Apr. 2014.

[54] J. Verrelst, L. Alonso, J. P. Rivera Caicedo, J. Moreno, and G. Camps-Valls, "Gaussian process retrieval of chlorophyll content from imaging spectroscopy data," *IEEE J. Sel. Topics Appl. Earth Observ. Remote Sens.*, vol. 6, no. 2, pp. 867–874, Apr. 2013, doi: 10.1109/JSTARS.2012.2222356.

[55] J. Verrelst, L. Alonso, G. Camps-Valls, J. Delegido, and J. Moreno, "Retrieval of vegetation biophysical parameters using Gaussian process techniques," *IEEE Trans. Geosci. Remote Sens.*, vol. 50, no. 5, pp. 1832–1843, May 2012, doi: 10.1109/TGRS.2011.2168962.

[56] D. R. Anderson, K. P. Burnham, and W. L. Thompson, "Null hypothesis testing: Problems, prevalence, and an alternative," *J. Wildlife Manage.*, vol. 64, no. 4, pp. 912–923, 2000, doi: 10.2307/3803199.

[57] F. Baret, S. Jacquemoud, G. Guyot, and C. Leprieur, "Modeled analysis of the biophysical nature of spectral shifts and comparison with information content of broad bands," *Remote Sens. Environ.*, vol. 41, no. 2, pp. 133–142, Aug. 1992, doi: 10.1016/0034-4257(92)90073-S.

[58] T. H. Rehman, A. F. Borja Reis, N. Akbar, and B. A. Linquist, "Use of normalized difference vegetation index to assess N status and predict grain yield in rice," *Agronomy J.*, vol. 111, no. 6, pp. 2889–2898, 2019, doi: 10.2134/agronj2019.03.0217.

[59] C. Buschmann, S. Lenk, and H. K. Lichtenthaler, "Reflectance spectra and images of green leaves with different tissue structure and chlorophyll content," *Isr. J. Plant Sci.*, vol. 60, nos. 1/2, pp. 49–64, May 2012, doi: 10.1560/IJPS.60.1-2.49.

[60] H. K. Lichtenthaler, "[34] chlorophylls and carotenoids: Pigments of photosynthetic biomembranes," in *Methods Enzymology*, vol. 148. New York, NY, USA: Academic, 1987, pp. 350–382, doi: 10.1016/0076-6879(87)48036-1.

[61] C. Banninger, "Phenological changes in the red edge shift of Norway spruce needles and their relationship to needle chlorophyll content," *ESA, Phys. Meas. Signatures Remote Sens.*, vol. 1, pp. 155–158, 1991.

[62] E. H. Murchie and T. Lawson, "Chlorophyll fluorescence analysis: A guide to good practice and understanding some new applications," *J. Exp. Botany*, vol. 64, no. 13, pp. 3983–3998, Oct. 2013, doi: 10.1093/jxb/ert208.
[63] Y. Ryu, J. A. Berry, and D. D. Baldocchi, "What is global photosynthesis? History, uncertainties and opportunities," *Remote Sens. Environ.*, vol. 223, pp. 95–114, Mar. 2019, doi: 10.1016/j.rse.2019.01.016.
[64] M. P. Cendrero-Mateo, A. E. Carmo-Silva, A. Porcar-Castell, E. P. Hamerlynck, S. A. Papuga, and M. S. Moran, "Dynamic response of plant chlorophyll fluorescence to light, water and nutrient availability," *Funct. Plant Biol.*, vol. 42, no. 8, pp. 746–757, 2015.
[65] S. Van Wittenberghe et al., "Towards the quantitative and physically-based interpretation of solar-induced vegetation fluorescence retrieved from global imaging," *Photosynthetica*, vol. 59, pp. 438–457, Jul. 2021, doi: 10.32615/ps.2021.034.
[66] I. Filella, A. Porcar-Castell, S. Munné-Bosch, J. Bäck, M. F. Garbulsky, and J. Peñuelas, "PRI assessment of long-term changes in carotenoids/chlorophyll ratio and short-term changes in de-epoxidation state of the xanthophyll cycle," *Int. J. Remote Sens.*, vol. 30, no. 17, pp. 4443–4455, Aug. 2009, doi: 10.1080/01431160802575661.
[67] A. Moncholi-Estornell, S. Van Wittenberghe, M. P. Cendrero-Mateo, L. Alonso, Z. Malenovský, and J. Moreno, "Impact of structural, photochemical and instrumental effects on leaf and canopy reflectance variability in the 500–600 nm range," *Remote Sens*, vol. 14, no. 1, Jan. 2022, Art. no. 56, doi: 10.3390/rs14010056.
[68] L. Gu, J. Han, J. D. Wood, C. Y.-Y. Chang, and Y. Sun, "Sun-induced chl fluorescence and its importance for biophysical modeling of photosynthesis based on light reactions," *New Phytologist*, vol. 223, no. 3, pp. 1179–1191, 2019, doi: 10.1111/nph.15796.
[69] N. C. Turner, E.-D. Schulze, and T. Gollan, "The responses of stomata and leaf gas exchange to vapour pressure deficits and soil water content," *Oecologia*, vol. 63, no. 3, pp. 338–342, Aug. 1984, doi: 10.1007/BF00390662.
[70] N. C. Parazoo et al., "Wide discrepancies in the magnitude and direction of modeled solar-induced chlorophyll fluorescence in response to light conditions," *Biogeosciences*, vol. 17, no. 13, pp. 3733–3755, Jul. 2020, doi: 10.5194/bg-17-3733-2020.
[71] C. van der Tol, J. A. Berry, P. K. E. Campbell, and U. Rascher, "Models of fluorescence and photosynthesis for interpreting measurements of solar-induced chlorophyll fluorescence," *J. Geophys. Res. Biogeosciences*, vol. 119, no. 12, Dec. 2014, Art. no. 2014JG002713, doi: 10.1002/2014JG002713.

M. Pilar Cendrero-Mateo received the Ph.D. degree in soil, water, and environmental sciences from the University of Arizona, Tucson, AZ, USA, in 2014.

She is currently a Researcher with the Imaging Processing Laboratory, Valencia, Spain. Her research interests include the use of ground-based spectroscopy techniques. This involves translating the biophysical properties of plants into measurable chlorophyll fluorescence and reflectance vegetation products. Her work includes experiments conducted at various scales, from controlled growth chambers and greenhouses to entire agricultural fields. Her overall goal is to understand the spatial and temporal variation of chlorophyll fluorescence and its role in remotely estimating the true photosynthetic efficiency of a plant.

Shari Van Wittenberghe received the Ph.D. degree in bioscience engineering from the University of Antwerp, Antwerp, Belgium, in 2014.

She is currently a Researcher with the Imaging Processing Laboratory, Valencia, Spain. Her research interests include on the hyperspectral monitoring of the dynamics of absorbed photosynthetic radiation at the leaf level, and how these dynamics are related to the controlled energy dissipation by the photosynthetic antenna. By working under both controlled and field conditions with current high spectral resolution sensors, the goal is to further improve the monitoring of photosynthetic light reactions leading to carbon sequestration from remote VIS-NIR hyperspectral observations.

Valero Laparra received the Ph.D. degree in computer science and mathematics from the Universitat de València, Valencia, Spain, in 2011.

He is currently an Assistant Professor with the Escola Tècnica Superior d'Enginyeria, Universitat de València, where he is also a Researcher with the Image Processing Laboratory. An important part of his research has focused on the development of state-of-the-art applications in the fields of manifold description, image processing (i.e., noise reduction, image quality evaluation, image compression, and image rendering), and rotation-based iterative Gaussianization methods.

Uwe Rascher received the Ph.D. degree in plant biology from the Technical University of Darmstadt, Darmstadt, Germany, in 2001.

He is currently the Head of the Shoot Dynamics research group at IBG-2, Forschungszentrum Jülich. He is an expert in the characterization of photosynthesis using chlorophyll fluorescence, hyperspectral reflectance, gas exchange, remote sensing and image analysis techniques. In his interdisciplinary work, he uses remote sensing to better quantify photosynthesis, to model plant-mediated leaf-to-region exchange, and to develop new concepts for field phenotyping. His current research interests include plant physiology, biogeochemistry, ecology, global climate change, and remote sensing.

Shirley A. Papuga received the Ph.D. degree in geological sciences from the University of Colorado, Boulder, CO, USA, in 2006.

She is currently an Associate Professor with the Department of Environmental Science and Geology, Wayne State University, Detroit, MI, USA. Her research interests include improving our understanding of ecohydrologic processes and their role in land surface-atmosphere interactions in natural and human-altered environments, particularly in the context of global change.

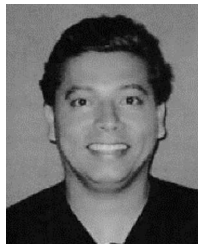

Guillermo Ponce-Campos received the Ph.D. degree in soil science from the University of Arizona, Tucson, AZ, USA, in 2011.

He is currently a Research Specialist with the McClaran Lab, University of Arizona. His main research interests include the analysis of satellite imagery to assess vegetation response to climate variability, and applying machine learning methods to the analysis of time series of satellite datasets.

Jose Moreno received the Ph.D. degree in theoretical physics from the University of Valencia, Valencia, Spain, in 1992.

He is currently a Professor of Earth Physics with the Department of Earth Physics and Thermodynamics, Faculty of Physics, University of Valencia, and the Director of the Earth Observation Image Processing Laboratory. His research interests include the modeling and monitoring of land surface processes using remote sensing techniques. He has participated in many international projects and research networks, as well as in the preparation and exploitation programs of several satellite missions.

Dr. Moreno has served as an Associate Editor of IEEE TRANSACTIONS ON GEOSCIENCE AND REMOTE SENSING and as a Guest Editor of the IEEE JOURNAL OF SELECTED TOPICS IN EARTH OBSERVATIONS AND REMOTE SENSING.